

Photon number correlation for quantum enhanced imaging and sensing

A. Meda¹, E. Losero^{1,2}, N. Samantaray¹, S. Pradyumna^{1,2},
A. Avella¹, I. Ruo-Berchera¹, M. Genovese^{1,3}

¹ INRIM, Strada delle Cacce 91, I-10135 Torino, Italy

² DISAT, Politecnico di Torino, I-10129 Torino, Italy

³ INFN Sezione di Torino, via P. Giuria 1, 10125, Torino, Italy

E-mail: i.ruoberchera@inrim.it

Abstract. In this review we present the potentialities and the achievements of the use of non-classical photon number correlations in many applications ranging from imaging to metrology. Photon number correlations in the quantum regime are easy to be produced and are rather robust against unavoidable experimental losses, and noise in some cases, if compared to the entanglement, where losing one photon can completely compromise the state and its exploitable advantage. Here, we will focus on quantum enhanced protocols in which only phase-insensitive intensity measurements (photon number counting) are performed, which allow probing transmission/absorption properties of a system, leading for example to innovative target detection schemes in a strong background. In this framework, one of the advantages is that the sources experimentally available emit a wide number of pairwise correlated modes, which can be intercepted and exploited separately, for example by many pixels of a Camera, providing a parallelism, essential in several applications, like wide field sub-shot-noise imaging and quantum enhanced ghost imaging. Finally, non-classical correlation enables new possibilities in quantum radiometry, e.g. the possibility of absolute calibration of a spatial resolving detector from the on-off- single photon regime to the linear regime, in the same setup.

1. Introduction

Quantum correlations are the subject of deep interest since their exploitation could open unprecedented opportunities in several fields, ranging from the very foundations of quantum mechanics [1] to cosmology [2, 3] and represent the basic resource for the development of quantum technologies as fundamental metrology [4, 5], quantum communication [6, 7], quantum biology [8, 9], quantum imaging and sensing [10, 11, 12, 13, 14].

Quantum enhanced measurement protocols aim at reducing the uncertainty in the estimation of some physical quantities of a system, related to some modification of an optical probe state, below classical shot noise limit (or standard quantum limit) scaling as $n^{-1/2}$, where n is the number of particles of the probe. Most theoretical investigations have been addressed to the use of entangled states to change this scaling with a stronger one, up to the ultimate limit imposed by quantum mechanics, n^{-1} , known as Heisenberg limit. Many measurement schemes have been proposed [15, 16], and some experimental proof of principle have been realized [17, 18, 19, 20, 21, 22, 23, 24] in this direction, typically using entangled state of the form $2^{-1/2}(|n0\rangle + |0n\rangle)$ (NOON state), where the n photons are distributed in the two paths of an interferometer accordingly. While two photon entangled states are quite routinely produced by post selected (double photon detection events) Spontaneous Parametric Down Conversion (SPDC) in very low gain regime, in practice generating and detecting $n > 2$ NOON state is really challenging. Even worse, entanglement itself is extremely fragile to the losses, for example loosing a single photon from a NOON state projects it in a classical mixture. Other quantum states, entangled and squeezed, have been considered, which are more resilient to experimental imperfections [25], but nevertheless reaching Heisenberg limit for a large number of photons, is probably a chimera. In fact, recently it has been shown that in presence of decoherence the Heisenberg limit and in general any chance of the uncertainty scaling with the photon number is out of reach [26, 27]. Rather, the enhancement with respect to the standard quantum limit is at most by constant factor, for example it takes the form $\sqrt{(1-\eta)/\eta}$ in presence of a loss factor $(1-\eta)$ [28, 29].

On the other side, the same advantage can be obtained more easily by exploiting non-classical Gaussian states [30], which are relatively easy to produce experimentally, such as squeezed vacuum generated by SPDC and Optical Parametric Oscillators (OPO). Single-mode squeezing [31, 32, 33, 34] in one of the quadratures (generated by OPO) has been the first quantum property considered for quantum metrology, in particular for enhanced interferometry [35] and the more successful from the practical point of view, leading to a real sensitivity improvement of the modern gravitational wave detectors [32, 36] and also to promising application to the photonic force microscopy for biological particle tracking [37, 38].

A fundamental property of two-mode squeezed vacuum, is that the state is entangled in the photon number basically assuming the form $\sum_{n=0}^{\infty} c_n |n\rangle |n\rangle$, meaning that two ideal detectors intercepting each modes respectively always measure the same

number of photon. This correlation is strongly non-classical and does not involve any measurement of the phase. Essentially, all the optical measurements, which aim at the estimation of an absorption, transmission and reflection can be enhanced by using photon number correlation. The idea is that one beam of the pair is used as a probe while the other acts as a reference, where the strong correlation helps in detecting slight modifications of the probe by some sort of comparison with the reference, a property that can be exploited from interferometry [39, 40] to imaging [1]. While the direct measurement of the photon number only, i.e. of the intensities, introduces some limitation in the field of applicability, it is experimentally more feasible in many situation, even in realistic scenario including noise and losses. It is emblematic in this framework, the possibility of detecting partially reflecting objects with significant enhanced sensitivity exactly when the background at the receiver is much more intense than the returning probe, just measuring non-classical photon number correlation [116].

These considerations can be extended to multi-mode spatial case. Indeed, when twin beams are produced through traveling wave parametric down conversion, or by four wave mixing in atomic vapors [42, 43, 44], the emission is approximatively a product of a large number of two-modes (spatial) squeezed states which can be intercepted and detected independently at the same time. Modern high sensitivity multi-pixel detectors, like CCD cameras can exploit this parallelism for improving the sensitivity of wide field imaging applications. For example one of the goal, which has been recently demonstrated is the possibility of realizing a new generation of wide field microscopes operating below the shot noise limit [45]. One of first application of SPDC entangled photons has been ghost imaging (GI)[46, 47], whose goal is the reconstruction of the spatial transmission/reflection profile of an object even if the photons interacting with it reach a single pixel detector. After GI as been demonstrated with classical correlation and even computational methods (exploiting random light pattern generated by a computer and spatial light modulator), nevertheless using non-classical correlation instead of classical ones can provide sensitivity advantage in very low illumination.

Finally, non-classical correlations have disclosed new possibilities in quantum radiometry [48], e.g. the possibility of absolute calibration of detectors, without the need of comparison with calibrated standards. The first proposal for calibrating single photon detector has been formulated by Klyshko [49] just after the discover of SPDC process and nowadays it is an established technique [50], currently used in metrological institutes. Generalizing the method to the domain of analog detectors and spatially resolving detector has lead recently to the first absolute calibration (of a EMCCD camera) from the on-off single photon regime to the linear regime, in the same setup, just changing the intensity of the SPDC pump laser.

One of the goal of this review is to give the reader all the elements for understanding with a certain level of detail the origin of the quantum advantage in the applications mentioned before, in particular linking clearly the sensitivity improvement with the degree of non-classicality measured by appropriate parameters. Since the losses are unavoidable in optical measurement and they usually affect quite a lot the performance

of quantum strategies, we always take them into consideration in the derivation of the results. The review is structured in this way. In Sec. 2 we introduce some basic elements of the quantum photodetection model. In Sec. 3 we discuss the non-classical photon statistics and photodetection statistics, how they can be quantified and the boundary between classical and quantum world. Sec. 4 presents in some detail the generation of photon-number entangled states in a spatially multi mode regime by SPDC and the issues related to the efficient detection of non-classical correlation in the far field of the emission. Following Sec.s 5-6-7-8 are devoted to the presentation of noticeable applications of quantum photon number correlations, in particular sub-shot noise imaging, target detection against a preponderant noise (quantum illumination), quantum enhanced ghost imaging and finally absolute calibration of detectors, respectively.

2. Quantum theory of photodetection

The quantum theory of photodetection was introduced by Glauber in 1965 [51]. The theory relates photocounts statistics to the intrinsic statistical nature of light. For centuries only thermal sources were available and the statistical description of light was confined to the Planck's distribution. Then, with the invention of the laser, a different statistical distribution, corresponding to the Poissonian distribution in the number of photons (as the one of an ensemble of independent particles) was observed [52]. This led to a theoretical effort to deeply understand the intrinsic statistical nature of different kinds of sources and how the process of the photodetection could affect it. Through photocounting rates is possible to estimate averages and fluctuations in the number of photons for different kind of radiations. Nevertheless, photodetection itself introduces randomness in the counting of the photon number due to the conversion of the illuminating field in a photocurrent; then, the relation between the photon statistics and the statistical properties of the process has to be considered.

According to quantum theory of photodetection, electromagnetic waves are quantized and the process of detection induces random losses in the number of photons that can be quantified in terms of the quantum efficiency η of the detection process. In little more in detail, the detection process of a field, using a linear photodetector, can be modelled as the random evolution of the field after passing through a beam splitter (BS) with transmission equal to η [53]. Introducing a bosonic annihilation operator \hat{a} , such that $[\hat{a}, \hat{a}^\dagger] = 1$. The unitary input - output relations of the BS provide the expression of the transmitted field \hat{b} of the single mode of an incoming field \hat{a} :

$$\hat{b}_1 = \sqrt{\eta} \hat{a} + i\sqrt{1-\eta} \hat{v} \quad (1)$$

$$\hat{b}_2 = \sqrt{1-\eta} \hat{v} + i\sqrt{\eta} \hat{a} \quad (2)$$

where \hat{v} is operator corresponding to the second input port of the BS, which is considered here in the vacuum state $|0\rangle$.

The photon statistics of the transmitted beams correspond to that of the input

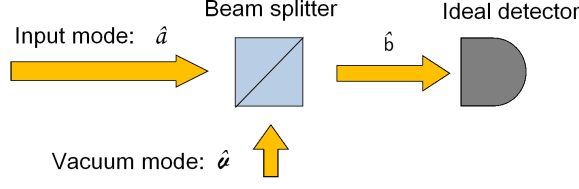


Figure 1. Model of a linear photodetector with quantum efficiency η corresponding to the transmissivity of the beam splitter.

beam after the random selection process has taken place. The evolution of the statistics of the number of photons of the incoming field, $\hat{n} = \hat{a}^\dagger \hat{a}$, can be easily calculated from Eq. (1) as:

$$\begin{aligned} \langle \hat{N} \rangle &= \langle \hat{b}_1^\dagger \hat{b}_1 \rangle = \eta \langle \hat{n} \rangle \\ \langle \Delta^2 \hat{N} \rangle &= \langle \hat{b}_1^\dagger \hat{b}_1 \hat{b}_1^\dagger \hat{b}_1 \rangle - \langle \hat{b}_1^\dagger \hat{b}_1 \rangle^2 = \eta^2 \langle \Delta^2 \hat{n} \rangle + \eta(1 - \eta) \langle \hat{n} \rangle \end{aligned} \quad (3)$$

where $\langle \hat{N} \rangle$ is the mean value of the measured photon number operator and $\langle \Delta^2 \hat{N} \rangle$ is its variance. In Eqs. 3, the definition of the quantum efficiency as the ratio between the detected and the incoming mean number of photons is recovered and the modification of the statistics when $\eta < 1$ is clearly expressed. Coherent states, with $\langle \Delta^2 \hat{n} \rangle = \langle \hat{n} \rangle$, and thermal states with $\langle \Delta^2 \hat{n} \rangle = \langle \hat{n} \rangle(1 + \langle \hat{n} \rangle)$, maintain the same statistical properties, just with a rescaled mean value. On the other side, losses in the detection process are the responsible of the degradation of sub-Poissonian statistics ($\langle \Delta^2 \hat{n} \rangle < \langle \hat{n} \rangle$), which is a signature of the quantum features of light as we will see in the Sec. 3. As a matter of fact, in the expression of the variance, the second term is a Poissonian noise, arising from the bosonic commutators, occurring even if the incoming field is without photon number fluctuation, ($\Delta^2 \hat{n} = 0$), for example a Fock state $|n\rangle$ eigenstate of the photon number operator. In presence of high losses ($\eta \ll 1$) the photocount statistics tends to the Poissonian one, vanishing the peculiar inner statistical properties of the field.

Also correlations are affected by the process of detection. Considering, for example, the covariance of two modes $\langle \Delta \hat{n}_1 \Delta \hat{n}_2 \rangle$, undergo two independent detection processes with quantum efficiencies η_1 and η_2 respectively, it evolves as

$$\langle \Delta \hat{N}_1 \Delta \hat{N}_2 \rangle = \eta_1 \eta_2 \langle \Delta \hat{n}_1 \Delta \hat{n}_2 \rangle.$$

3. Non-Classical Photon Statistics

Ideal photodetection, with no losses, is a measurement of the intrinsic statistical nature of light. The analysis of the fluctuation in the photon number can be used to trace a discrimination between the quantum and classical nature of the light, where the boundary is represented by the coherent states [51, 54, 55].

Coherent states, the one emitted by an ideal laser, correspond to a displaced ground state of the vacuum state:

$$|\alpha\rangle = D(\alpha)|0\rangle = \exp(\alpha\hat{a}^\dagger - \alpha^*\hat{a})|0\rangle \quad (4)$$

and are eigenstate of the annihilation operator, $\hat{a}|\alpha\rangle = \alpha|\alpha\rangle$, where α is complex number. In the photon number basis, the single mode state $|\alpha\rangle$ can be expressed as:

$$|\alpha\rangle = e^{|\alpha|^2/2} \sum_{n=0}^{\infty} \frac{\alpha^n}{\sqrt{n!}} |n\rangle \quad (5)$$

from which is possible to calculate the photon number distribution $p(n)$, that turns out to be Poissonian:

$$p(n) = |\langle \hat{n} | \alpha \rangle|^2 = e^{-\langle \hat{n} \rangle^2} \frac{\langle \hat{n} \rangle^n}{n!} \quad (6)$$

with photon-number variance equal to the mean photon number, $\langle \Delta^2 \hat{n} \rangle = \langle \hat{n} \rangle$. The uncertainty in the mean photon number $\Delta \hat{n} / \langle \hat{n} \rangle = 1 / \sqrt{\langle \hat{n} \rangle}$ is the so called “shot-noise level”. Poissonian fluctuation, or equivalently the shot noise level, represents indeed the lower bound for classical fields. This point can be clarified through the Glauber-Sudarshan representation [54, 56, 57]. Since coherent states phase and modulus completely span the phase-space (actually they form an over complete base) any arbitrary state with density matrix ρ , can be represented as a weighted combination of coherent states

$$\rho = \int d^2\alpha P(\alpha) |\alpha\rangle \langle \alpha|, \quad (7)$$

where $P(\alpha)$ is a quasi-probability distribution. Because ρ is Hermitian and has unit trace, $P(\alpha)$ is real and normalized to the unity. However, it not always behaves as a well defined probability density, for example can assume negative values or can be more singular than a delta function. Are considered classical state of light the ones having $P(\alpha) \geq 0$, then representing a true probability density function. This definition is motivated by the fact that for such states the photon statistics predicted by the quantum photodetection theory coincide with the one derived in the framework of the semiclassical theory of photodetection, where the incoming field is considered as classical wave [58, 59, 60] and the shot noise is the result of a random process due to the discreteness of the electron charge [61, 62] generated inside the detector (for all the three paradigms of direct, homodyne and heterodyne detection).

From Eq. (7), it follows that quantum expectation values of normally ordered operators are expressed through the integral of the corresponding classical quantities weighted with the quasi-probability distributions, as

$$\langle (\hat{a}^\dagger)^m (\hat{a})^n \rangle = \int d^2\alpha P(\alpha) (\alpha^*)^m \alpha^n \quad (8)$$

In particular, the expression of the photon-number variance within the Glauber-Sudarshan representation is [57]:

$$\langle \Delta^2 \hat{n} \rangle = \langle \hat{a}^\dagger \hat{a} \rangle + \langle (\hat{a}^\dagger)^2 (\hat{a})^2 \rangle - \langle \hat{n} \rangle^2 = \langle \hat{n} \rangle + \int d^2\alpha P(\alpha) (|\alpha|^2 - \langle |\alpha|^2 \rangle)^2 \quad (9)$$

and shows a first term due to the discreteness nature of the light, the shot noise, and a second term that can be interpreted as a quasi-classical variance. For classical states, with $P(\alpha) \geq 0$, the integral is positive or null, and the fluctuations are Poissonian or super-Poissonian. For non-classical states, in which the quasi-probability assumes negative value (single photons, squeezed states, or entangled state) it is possible to have a negative integral, allowing sub shot noise fluctuations.

The definition of classical state according to its statistical properties, as expressed in Eq. (9), can be also expressed considering the Fano factor $F = \langle \Delta^2 \hat{n} \rangle / \langle \hat{n} \rangle$ [63] or the Mandel's Q parameter [64]:

$$Q = \frac{\langle \Delta^2 \hat{n} \rangle - \langle \hat{n} \rangle}{\langle \hat{n} \rangle} = F - 1 \quad (10)$$

The Fano factor $F = 1$ ($Q = 0$) establishes a bound between classical and non-classical photon statistics; F lower bounded by the unity for classical states, while specific non-classical states can have $0 \leq F < 1$ ($-1 \leq Q < 0$).

As pointed out in Section 2, the statistics of a state are deteriorated by the losses in the photodetection process (including both losses in the optical path and the detector quantum efficiency). The Fano factor in presence of optical losses η becomes $F_{det} = \eta F + 1 - \eta$, as it descends from Eq. (3). Thus, the lower bound allowed to the non-classicality in presence of losses is $F_{det} = 1 - \eta$.

3.1. Two mode non-classical statistics

In analogy to Eq. (7), a classical two-mode (bipartite) state is represented by a Glauber-Sudarshan probability density function $P(\alpha_1, \alpha_2) \geq 0$

$$\rho_{1,2} = \int d^2\alpha_1 d^2\alpha_2 P(\alpha_1, \alpha_2) |\alpha_1\rangle |\alpha_2\rangle \langle \alpha_1| \langle \alpha_2|. \quad (11)$$

Considering two fields with mean detected photon number N_1 and N_2 , we can quantify the degree of correlation between the modes and its non-classical features defining the noise reduction factor σ as the ratio between the variance of the difference in the number of photons, normalized to the noise of two subtracted coherent states [65, 66, 67, 68, 69, 70, 72, 73, 74, 75]:

$$\sigma = \frac{\langle \Delta^2(\hat{n}_1 - \hat{n}_2) \rangle}{\langle \hat{n}_1 + \hat{n}_2 \rangle} = \frac{\langle \Delta^2 \hat{n}_1 \rangle + \langle \Delta^2 \hat{n}_2 \rangle - 2\langle \Delta \hat{n}_1 \Delta \hat{n}_2 \rangle}{\langle \hat{n}_1 + \hat{n}_2 \rangle} \quad (12)$$

The noise reduction factor represents the equivalent of the Fano factor for a bipartite state; in this case, the shot noise level is given by the sum of the shot noise of the two modes $\langle \hat{n}_1 + \hat{n}_2 \rangle$. For classical bipartite states, σ is lower bounded by 1, while for non classical beams quantum correlations can lead to $0 \leq \sigma < 1$. Also in this case the limit in the reduction of σ is represented by the losses. From Eq. (3), considering two modes subject to the same transmission-detection efficiency $\eta_1 = \eta_2 = \eta$,

$$\sigma_{det} = \eta\sigma + 1 - \eta. \quad (13)$$

The lower bound in presence of losses is therefore $\sigma_{det} = 1 - \eta$.

A demonstration of the classical limit of the correlation can be easily achieved in a specific case. Let us consider a two mode state generated by splitting a single mode \hat{a} with a beam splitter of transmittance τ . In the case of ideal photodetection, the statistics of the output modes can be computed using the input-output relations of the BS in Eq.s (1) (with $\tau = \eta$) as:

$$\langle \Delta^2 \hat{n}_1 \rangle = \langle \hat{b}_1^\dagger \hat{b}_1 \hat{b}_1^\dagger \hat{b}_1 \rangle - \langle \hat{b}_1^\dagger \hat{b}_1 \rangle^2 = \tau^2 \langle \Delta^2 \hat{n} \rangle + \tau(1 - \tau) \langle \hat{n} \rangle \quad (14)$$

$$\langle \Delta^2 \hat{n}_2 \rangle = \langle \hat{b}_2^\dagger \hat{b}_2 \hat{b}_2^\dagger \hat{b}_2 \rangle - \langle \hat{b}_2^\dagger \hat{b}_2 \rangle^2 = (1 - \tau)^2 \langle \Delta^2 \hat{n} \rangle + \tau(1 - \tau) \langle \hat{n} \rangle$$

$$\langle \Delta \hat{n}_1 \Delta \hat{n}_2 \rangle = \langle \hat{b}_1^\dagger \hat{b}_1 \hat{b}_2^\dagger \hat{b}_2 \rangle - \langle \hat{b}_1^\dagger \hat{b}_1 \rangle \langle \hat{b}_2^\dagger \hat{b}_2 \rangle = \tau(1 - \tau) [\langle \Delta^2 \hat{n} \rangle - \langle \hat{n} \rangle] \quad (15)$$

The last expression reveals that in order to have a non-null covariance the statistics of the incoming light must be super-poissonian, which also means that a split coherent state does not generate any correlation, while a thermal beam does. Using the relations (14-15) into Eq. (12) one can express the noise reduction factor as:

$$\sigma = (F - 1)(2\tau - 1)^2 + 1 \quad (16)$$

where $F = \langle \Delta^2 \hat{n} \rangle / \langle \hat{n} \rangle$. For a balanced 50 - 50 ($\tau = 1/2$) beam splitter this leads to the classical limit $\sigma = 1$, irrespective to the statistical properties of the incoming beam, either sub-poissonian or super-poissonian. This means that the correlated super-poissonian fluctuations of the two modes are suppressed in the subtraction, except the shot noise. On the other side, for unbalanced beam splitter, i.e. $\tau \neq 1/2$, an incoming field with sub-poissonian statistics generates non-classical correlations at the output ports.

Another parameter that can be used as an indicator of non classicality for two mode states is the Cauchy-Schwarz parameter [76]:

$$\varepsilon = \frac{\langle : \Delta \hat{n}_1 \Delta \hat{n}_2 : \rangle}{\sqrt{\langle : \Delta \hat{n}_1 : \rangle \langle : \Delta \hat{n}_2 : \rangle}} \quad (17)$$

where $\langle : \rangle$ is the normally ordered quantum expectation value. While σ is deteriorated by the losses, ε is remarkably immune to them and for this reason it allows accessing experimentally to the non classical features, even for inefficient detection process. However, noise added to the detection degradate its value. For classical states of light, with a positive Glauber-Sudarshan P function, the Cauchy-Schwarz parameter is equal to one, while for states with a negative (or singular) P function the limit $\varepsilon = 1$ can be violated. In the case of correlated thermal beams, obtained by a 50:50 BS, the most used classically correlated states (see, for example, the classical ghost imaging protocols), the $\langle : \Delta^2 \hat{n}_1 : \rangle_{TH} = \langle : \Delta^2 \hat{n}_2 : \rangle_{TH} = \langle \Delta \hat{n}_1 \Delta \hat{n}_2 \rangle_{TH} = \langle \hat{n} \rangle^2$, as can be simply derived by Eq. (15-15), by introducing the thermal variance $\langle \Delta^2 \hat{n} \rangle = \langle \hat{n} \rangle(1 + \langle \hat{n} \rangle)$. The Cauchy-Schwarz parameter for a split thermal beam is $\varepsilon_{TH} = 1$ saturating the classical bounds. This demonstrates that thermal split beams show the best possible correlation allowed for classical states. They represent the classical benchmark for comparing the quantum enhanced performance in some emblematic imaging and sensing protocols, see Sec. 6 and 7.

4. Spatially Multi-Mode Photon Number Correlation: Generation and Detection

Actually, the most efficient ways to produce quantum correlations between optical fields are based on SPDC [77, 78]. This physical phenomenon was discovered at the end of sixties [49, 79] and in recent years, thanks to the development of new kinds of laser systems and photon detectors, it is exploited in the most advanced quantum technologies like quantum key distribution [80, 81, 82, 83, 84, 85], quantum computing [86, 87, 88, 89, 90], tailoring of quantum states [91, 92, 93], quantum imaging [13, 94] and quantum sensing [95]. Moreover, SPDC is exploited in several experiment concerning the foundation of quantum mechanics [96, 97, 98, 99]. SPDC is due to the interaction between an intense optical field, usually called pump beam, and a non-linear optical medium. Basically, the phenomenon consists in the decay of one photon into two photons preserving energy and momentum:

$$\begin{aligned}\omega_0 &= \omega_1 + \omega_2 \\ \mathbf{k}_0 &= \mathbf{k}_1 + \mathbf{k}_2\end{aligned}\tag{18}$$

where ω_0 is the frequency of the *pump photon* and ω_1, ω_2 are the frequencies of the photons emitted by SPDC, and where k_j (with $j=0,1,2$) are the corresponding wave vectors (see Fig.2).

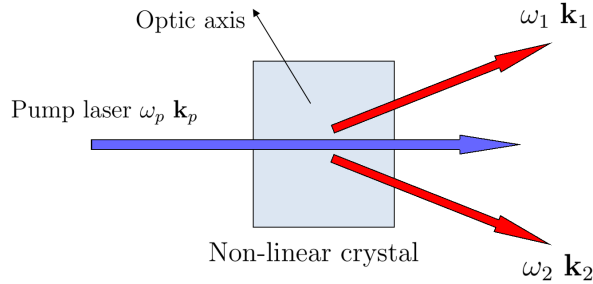


Figure 2. Schematic representation of the spontaneous parametric down conversion.

In this chapter we will see a brief introduction on the physics of the SPDC process. Moreover, we will derive the SPDC photons statistics in order to quantify the quantum correlations.

4.1. Spontaneous Parametric Down Conversion

In non-linear optics, the dielectric polarization P is expanded as

$$P = \chi^1 E + \chi^2 EE + \chi^3 EEE + \dots\tag{19}$$

For higher strength of the electric field (E), the higher order non linear terms becomes important. Except χ^1 being the linear susceptibility coefficient, χ^2 and χ^3 are called non linear susceptibility coefficient of the medium. Taking into accounts non-linear effects

until the second order, the field Hamiltonian in a non-magnetic medium can be written as

$$H(t) = \int_V \left[\frac{B^2(r, t)}{2\mu_0} + \frac{1}{2}\epsilon_0 E^2(r, t) + X_1(r, t) + X_2(r, t) \right], \quad (20)$$

where,

$$X_1(r, t) = \frac{1}{2}\chi_{i,j}^1 E_i E_j \quad (21)$$

and

$$X_2(r, t) = \frac{1}{3}\chi_{i,j,k}^2 E_i E_j E_k. \quad (22)$$

The last expression represents the non-linear interaction involving three electric fields and it is responsible for two of the most important optical non-linear process: the Second Harmonic Generation (SHG) and the PDC. We are interested in the last one to which corresponds the following interaction Hamiltonian:

$$H_I(t) = \frac{1}{3} \int_V \chi_{i,j,k}^2 E_i E_j E_k dV, \quad (23)$$

here the interaction extends over the volume V of the non-linear medium. Even in case of strong non linearity and high rate of pairs production, the probability that a pump photon is down converted is very low. The pump should be very intense and it is treated classically whereas the quantum description of the down converted pairs is essential. The electric field of a down converted pairs can be written in quantized form as

$$\hat{E}_j(\mathbf{r}, t) \propto \int \int \left[\hat{a}_j(\mathbf{k}_j) e^{i(\mathbf{k}_j \mathbf{r} - \omega_j t)} + H.C. \right] d^3 k_j d\omega_j, \quad (24)$$

where the indexes can be $j = 1, 2$. The electric field of a monochromatic pump propagating along Z axis direction is

$$E_p(\mathbf{r}, t) = A_p(\boldsymbol{\rho}) e^{i(\mathbf{k}_p \mathbf{z} - \omega_p t)} \quad (25)$$

where, $\boldsymbol{\rho}$ is the coordinate vector in the transverse X-Y plane. For simplicity, each wave vector can be divided into the longitudinal component (pump direction), k_{jz} and transverse component, \mathbf{q}_j . With these consideration for the three interacting fields, the interaction Hamiltonian becomes:

$$H_I(t) = \int \int \int g A_p(\boldsymbol{\rho}) \hat{a}_{k_1}^\dagger \hat{a}_{k_2}^\dagger e^{i(k_p - k_{1,z} - k_{2,z})z} e^{i(\mathbf{q}_1 + \mathbf{q}_2)\boldsymbol{\rho}} \times e^{-i(\omega_p - \omega_1 - \omega_2)t} dz d\omega_1 d\omega_2 d^2 q_1 d^2 q_2 d^2 \rho \quad (26)$$

where g is a coupling constant depending by χ^2 . Initially the down converted fields are in the vacuum state, and upon the interaction, the evolved state in the Schrödinger picture follows

$$|\psi\rangle = \exp \left[-\frac{1}{i\hbar} \int H_I(t') dt' \right] |0\rangle \quad (27)$$

Solving the time integral and considering a constant χ^2 , Dirac delta function is obtained recovering $\omega_p = \omega_1 + \omega_2$. Considering the L , the length of the crystal the the space integral in the z direction is

$$\int_0^L e^{i(k_p - k_{1z} - k_{2z})z} dz = L e^{i\Delta k z/2} \text{sinc}(\Delta k L/2), \quad (28)$$

where $\Delta k = k_p - k_{1z} - k_{2z}$ being the longitudinal phase mismatch. In the limit $L \rightarrow \infty$, the sinc function becomes a delta function and the integral term is different from zero for perfect phase matching condition, i.e $\Delta k = 0$. In the realistic situation, finite thickness of the crystal induces phase mismatch, whose measure is given by the width of the sinc central peak.

Similar considerations can be performed on the interaction time T . The integral on time interaction of Eq. (27) leads to:

$$\int_0^T e^{-i(\omega_p - \omega_1 - \omega_2)t} dt = T e^{-i\Delta\omega T/2} \text{sinc}(\Delta\omega T/2), \quad (29)$$

where $\Delta\omega = \omega_p - \omega_1 - \omega_2$ is the frequency phase mismatch. Also in this case, in the limit $T \rightarrow \infty$ (i.e. plane wave), the sinc function becomes a delta function and the integral term is different from zero for perfect phase matching condition, i.e $\Delta\omega = 0$.

If we consider the pump as a plane wave, infinite width of the pump and the crystal in the transverse direction of propagation leads to the surface integral

$$\int_S e^{i(\mathbf{q}_1 + \mathbf{q}_2) \cdot \boldsymbol{\rho}} d^2\rho = \delta(\mathbf{q}_1 + \mathbf{q}_2), \quad (30)$$

moreover we have $\Delta\omega = 0$ and $A_p(\boldsymbol{\rho}) = A_0$ with A_0 constant. In this approximation, the down converted modes are perfectly correlated in the transverse direction, i.e the signal modes with transverse momenta \mathbf{q} is correlated to the corresponding idler momenta $(-\mathbf{q})$. With this simplification, the evolution operator becomes:

$$\hat{S} = \exp \left[\int \left(f(\mathbf{q}, \Omega) \hat{a}_{\mathbf{q}, \Omega}^\dagger \hat{a}_{-\mathbf{q}, -\Omega}^\dagger - H.C. \right) d^2q d\omega \right] \quad (31)$$

where $f(\mathbf{q}, w)$, contains the information about the interacting fields and the non-linear medium:

$$f(\mathbf{q}, w) = A_0 L e^{i\Delta z/2} \text{sinc} \left(\frac{\Delta k(\mathbf{q}, w) L}{2} \right)$$

and the modes are identified by a frequencies $\omega_p/2 \pm \Omega$ and transverse momenta $\pm \mathbf{q}$. The quantum state of SPDC modes at the start of the process is a vacuum state, due to the time evolution becomes:

$$|\psi\rangle = \exp \left[\int \left(f(\mathbf{q}, w) \hat{a}_{\mathbf{q}, \Omega}^\dagger \hat{a}_{-\mathbf{q}, -\Omega}^\dagger - H.C. \right) d^2q d\omega \right] |0\rangle, \quad (32)$$

Considering discrete values of q , w , the integral can be replaced by the summation

$$|\psi\rangle = \exp \left[\sum_{\mathbf{q}, \Omega} f(\mathbf{q}, \Omega) \hat{a}_{\mathbf{q}, \Omega}^\dagger \hat{a}_{-\mathbf{q}, -\Omega}^\dagger - H.C. \right] |0\rangle \quad (33)$$

Since the modes corresponding to different variables commute with each other, following the BCH relation, i.e $e^{x(\hat{A}+\hat{B})} = e^{x\hat{A}} \cdot e^{x\hat{B}}$ for $[\hat{A}, \hat{B}] = 0$, the above state can be written in the direct product form as follows

$$|\psi\rangle = \bigotimes_{\mathbf{q}, \Omega} \exp \left[f(\mathbf{q}, \Omega) \hat{a}_{\mathbf{q}, \Omega}^\dagger \hat{a}_{-\mathbf{q}, -\Omega}^\dagger - H.C. \right] |0\rangle \quad (34)$$

Thus, performing the series expansion of the exponential, it is possible to see that the generated SPDC state naturally represents a multi mode structure. The state resembles to the direct product of twin beam states $|TWB\rangle = \sum_{n=0}^{\infty} c_n |n, n\rangle_{1,2}$, whose transverse momenta are perfectly correlated.

$$|\psi\rangle = \bigotimes_{\mathbf{q}, \Omega} |TWB\rangle_{\mathbf{q}, \Omega} = \bigotimes_{\mathbf{q}, \Omega} \sum_n c_{\mathbf{q}, \Omega}(n) |n\rangle_{\mathbf{q}, \Omega_s} |n\rangle_{-\mathbf{q}, -\Omega} \quad (35)$$

Where the probability amplitude $c_{\mathbf{q}, \Omega}(n) \propto \sqrt{\mu^n / (\mu + 1)^{n+1}}$ is a coefficient that can be considered constant and it is related to the mean number of photons per mode μ .

4.2. SPDC photon statistics

We are now interested in the statistical distribution of photons for a couple of conjugated modes, indicated by $\hat{a}_{(\mathbf{q}, \Omega)} \rightarrow \hat{a}_1$ and $\hat{a}_{(-\mathbf{q}, -\Omega)} \rightarrow \hat{a}_2$. To calculate this it is convenient to consider the evolution operator (the so called two-mode squeezing operator):

$$\hat{S}_{1,2} = \exp \left[f(\mathbf{q}, \Omega) \hat{a}_1^\dagger \hat{a}_2^\dagger - H.C. \right] \quad (36)$$

acting only on conjugated modes. For simplicity, we rewrote the complex amplitude as $f(\mathbf{q}, \Omega) = r e^{i\theta}$ where $r(\mathbf{q}, \Omega) = A_0 L \operatorname{sinc} \left(\frac{\Delta k(\mathbf{q}, w) L}{2} \right)$ and $\theta(\mathbf{q}, \Omega) = \Delta k z / 2$. The real quantity r is usually referred as to squeezing parameter. Following the BCH relation, the input-output relation for mode 1 and mode 2 follows as

$$\hat{S}_{1,2}^\dagger \hat{a}_1 \hat{S}_{1,2} = U_1 \hat{a}_1 + V_1 \hat{a}_2^\dagger \quad (37)$$

$$\hat{S}_{1,2}^\dagger \hat{a}_2 \hat{S}_{1,2} = U_2 \hat{a}_2 + V_2 \hat{a}_1^\dagger, \quad (38)$$

where:

$$U_1 = \cosh(r), \quad (39)$$

$$V_1 = e^{i\theta} \sinh(r), \quad (40)$$

$$U_2 = \cosh(r), \quad (41)$$

$$V_2 = e^{i\theta} \sinh(r). \quad (42)$$

Now, we are able to calculate the mean photon number per mode:

$$\begin{aligned} \mu = \langle \hat{n}_1 \rangle = \langle \hat{n}_2 \rangle &= \langle \hat{a}_j^\dagger \hat{a}_j \rangle = \langle 0, 0 | \hat{S}^\dagger \hat{a}_j^\dagger \hat{a}_j \hat{S} | 0, 0 \rangle \\ &= \langle 0, 0 | \hat{S}^\dagger \hat{a}_j^\dagger \hat{S}^\dagger \hat{S} \hat{a}_j \hat{S} | 0, 0 \rangle \\ &= \langle 0, 0 | \left[\hat{a}_1^\dagger \cosh(r) + \hat{a}_2 \sinh(r) e^{-i\theta} \right] \times \\ &\quad \times \left[\hat{a}_1 \cosh(r) + \hat{a}_2^\dagger \sinh(r) e^{i\theta} \right] | 0, 0 \rangle \\ &= \sinh^2(r). \end{aligned} \quad (43)$$

where the index $j=1,2$ denote the two conjugated modes. The unitary condition $\hat{S}^\dagger \hat{S} = 1$ is used in Eq. (43) in passing from step one to two.

It is possible deriving the statistical momenta of superior orders by following the same steps as in the previous calculation. In particular we are interested in:

$$\begin{aligned} \langle : \hat{n}_1 \hat{n}_2 : \rangle &= \langle \hat{a}_1^\dagger \hat{a}_2^\dagger \hat{a}_1 \hat{a}_2 \rangle = \sinh^2(r) \cosh^2(r) + \sinh^4(r) \\ &= 2\mu^2 + \mu. \end{aligned} \quad (44)$$

$$\langle : \hat{n}_1 \hat{n}_1 : \rangle = \langle : \hat{n}_2 \hat{n}_2 : \rangle = 2 \sinh^4(r) = 2\mu^2 \quad (45)$$

and

$$\begin{aligned} \langle (\Delta \hat{n}_1)^2 \rangle &= \langle : \hat{n}_1 \hat{n}_1 : \rangle - \langle \hat{n}_1 \rangle^2 + \langle \hat{n}_1 \rangle \\ &= \langle \hat{n}_1 \rangle (1 + \langle \hat{n}_1 \rangle) = \mu(1 + \mu) = \langle (\Delta \hat{n}_2)^2 \rangle \end{aligned} \quad (46)$$

$$\begin{aligned} \langle : \Delta \hat{n}_1 \Delta \hat{n}_2 : \rangle &= \langle : \hat{n}_1 \hat{n}_2 : \rangle - \langle \hat{n}_1 \rangle \langle \hat{n}_2 \rangle \\ &= \langle \hat{n}_1 \rangle (1 + \langle \hat{n}_1 \rangle) = \langle \hat{n}_2 \rangle (1 + \langle \hat{n}_2 \rangle) = \mu(1 + \mu) \end{aligned} \quad (47)$$

4.3. Detected photon statistics

Above we have derived the statistical behaviour of SPDC photons emitted in two conjugated modes. Here we are interested in the statistical behaviour of the detected photons on two detectors, each of them collecting the photons emitted in one of the two conjugated modes.

According to the simple detection model of Sec.2 and the results of Sec.4.2, it easily follows that:

$$\langle \hat{N}_j \rangle = \eta_j \langle \hat{a}_j^\dagger \hat{a}_j \rangle = \eta_j \mu \quad (48)$$

$$\langle (\Delta \hat{N}_j)^2 \rangle = \eta_j^2 \mu^2 + \eta_j \mu \quad (49)$$

and the covariance

$$\langle : \Delta \hat{N}_1 \Delta \hat{N}_2 : \rangle = \eta_1 \eta_2 \mu (1 + \mu) \quad (50)$$

Now it is possible to calculate the parameters that quantify the degree of correlation between two modes, like the noise reduction factor σ defined in Eq. (12). As described in Sec. 3.1, the noise reduction factor is an important parameter because allows discriminating between classical states of light and quantum states of light. If $\sigma \geq 1$ we are in presence of classical light like thermal light or coherent light, if $\sigma < 1$ we have quantum correlated light.

Applying the statistical behaviour of two conjugated modes of SPDC, calculated in this chapter, from the definition of Eq. (12) we obtain:

$$\sigma = 0 \quad (51)$$

and therefore for Eq. (13) we have:

$$\sigma_{det} \simeq 1 - \eta \quad (52)$$

where we assumed $\eta_1 = \eta_2 = \eta$. For unbalanced losses, the noise reduction factor can be expressed as:

$$\sigma_{det} = 1 - \bar{\eta} + \frac{(\eta_1 - \eta_2)^2}{2\bar{\eta}} \left(\mu + \frac{1}{2} \right), \quad (53)$$

where μ is the mean number of photons per mode and $\bar{\eta}$ is the mean quantum efficiency. Eq 52 shows how the measured noise reduction factor between two conjugated modes is always smaller than 1 in the case of symmetrical quantum efficiency. Otherwise, if we have $\eta_1 \neq \eta_2$ there is an additional term, usually called excess noise, that is always positive and can lead to measure $\sigma > 1$ even in case of perfectly correlated quantum light.

These results are valid in the plane wave pump approximation. In experiments the momentum distribution of the pump, which can not be a delta function, generates an uncertainty in the relative momentum (direction of propagation) of correlated photons. Therefore, a full study of the modes collection inside finite detection areas is needed.

4.4. Modes collection in the far field

In the far field region, obtained at the focal plane of a thin lens in a $f - f$ configuration, any transverse mode \mathbf{q} is associated with a single position \mathbf{x} according to the geometric transformation $(2cf/\omega)\mathbf{q} \rightarrow \mathbf{x}$, where c is the speed of light. The exact condition $\mathbf{q}_1 + \mathbf{q}_2 = 0$ for correlated photons, which comes from the integral in Eq. (30) in the plane wave pump approximation, becomes in the far field a strict condition on the their positions, $\mathbf{x}_1 + \mathbf{x}_2 = 0$. For degenerate frequency, $\omega_1 = \omega_2 = \omega_p/2$, correlated photon reach symmetric position with respect to the pump intersection point ($\mathbf{x} = 0$). A more realistic Gaussian distributed pump with angular spread $\Delta\mathbf{q}$ leads to an uncertainty on the position of correlated photon, $\mathbf{x}_1 + \mathbf{x}_2 = 0 \pm \Delta\mathbf{x}$, where $\Delta\mathbf{x} = (2cf/\omega_p)\Delta\mathbf{q}$ represents the size, in the far field, of the coherence area \mathcal{A}_{coh} in which it is possible to collect photons from correlated modes. It is possible to visualise coherence areas in the high gain regime ($r > 1$) where they appear like correlated spots (speckles) around symmetrical positions \mathbf{x} and $-\mathbf{x}$, where the center of symmetry (CS) is basically the pump-detection plane interception. These correlations in photon numbers can be appreciated in Fig. 3.

It is possible to measure the size of this of the coherence area by performing the spatial cross-correlation between the two beams:

$$c(\xi) = \sum_{\mathbf{x}} \frac{\langle \delta \hat{N}_1(\mathbf{x}) \delta \hat{N}_2(-\mathbf{x} + \xi) \rangle}{\sqrt{\langle [\delta \hat{N}_1(\mathbf{x})]^2 \rangle \langle [\delta \hat{N}_2(-\mathbf{x} + \xi)]^2 \rangle}}$$

where $\xi = (x, y)$ is the shift.

It is obvious that, in order to collect most of the correlated photons, two symmetrically placed detectors must have sensitive areas A_{det} larger than the coherence area A_{coh} . Referring to Fig. 4 we collect photons over two equal and symmetric areas

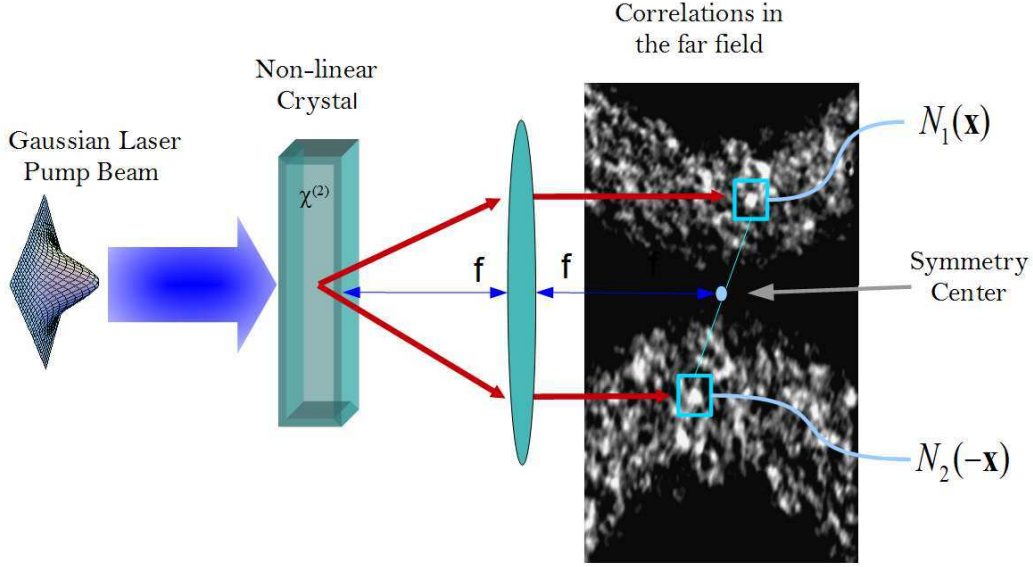


Figure 3. Far field emission of TYPE II SPDC in the non-linear high gain regime, in which super-poissonian fluctuation is responsible for the speckled structure. The rings showed correspond to a spectral selection of $10nm$ around the degeneracy.

$\mathcal{A}_{det,j}$ ($j = 1, 2$) containing a large number of transverse spatial modes $\mathcal{M}_c = A_{det,j}/A_{coh}$, and for a time sufficient to collect many temporal modes $\mathcal{M}_t = \mathcal{T}_{det}/\mathcal{T}_{coh}$. However, there are modes \mathcal{M}_b on the border of the detectors which are only partially detected, namely with efficiency β that can be assumed equal to $1/2$ on average. Moreover, experimental misalignment can leads to collect some uncorrelated modes \mathcal{M}_u . Even if it is possible to optimise the experiment in order to have a small contribution of \mathcal{M}_b and \mathcal{M}_u , anyway it is necessary to take them into account in the model.

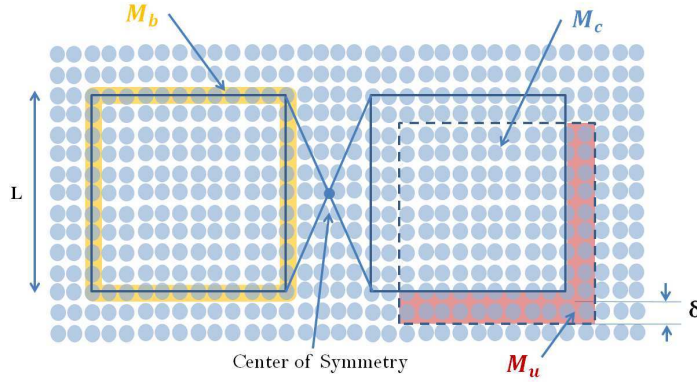


Figure 4. A scheme of the correlated modes \mathcal{M}_c , the uncorrelated \mathcal{M}_u and the partially correlated modes \mathcal{M}_b , when we assume to have a misalignment with respect to the center of simmetry (CS) indicated by the blue dot

Since each SPDC mode is independent, the variance and covariance of a state with \mathcal{M} pairs are \mathcal{M} times the values of a single pair. Therefore, taking into account the

contribution of the different kind of modes involved, and the single/two mode statistics in Eq. (48,49,50) one has:

$$\langle \hat{N}_j \rangle = \mathcal{M}_{tot} \eta_j \mu \quad (54)$$

$$\langle (\delta \hat{N}_j)^2 \rangle = \mathcal{M}_{tot} \eta_j \mu (1 + \eta_j \mu) \quad (55)$$

and considering the different modes contribution:

$$\langle \hat{N}_j \rangle = (\mathcal{M}_c + \mathcal{M}_u + \mathcal{M}_b \beta) \eta_j \mu \quad (56)$$

$$\langle (\delta \hat{N}_j)^2 \rangle = (\mathcal{M}_c + \mathcal{M}_u) \eta_j \mu (1 + \eta_j \mu) + \mathcal{M}_b \beta \eta_j \mu (1 + \beta \eta_j \mu) \quad (57)$$

$$\langle \delta \hat{N}_1 \delta \hat{N}_2 \rangle = (\mathcal{M}_c + \mathcal{M}_b \beta^2) \eta_1 \eta_2 \mu (1 + \mu). \quad (58)$$

where μ is the mean photon number per mode, η_1 and η_2 are the detection efficiencies of signal and idler beam respectively.

Substituting the previous expressions into the definition of the noise reduction factor in Eq. (12) leads:

$$\sigma_{det} \simeq 1 - \eta A \quad (59)$$

The quantity $0 < A < 1$ can be interpreted as a collection efficiency of correlated photons pairs (or modes) and assumes the form:

$$A = (\mathcal{M}_c + \mathcal{M}_b \beta^2 - \mathcal{M}_u \mu) / (\mathcal{M}_c + \mathcal{M}_u + \mathcal{M}_b \beta) \quad (60)$$

It is possible to evaluate this collection efficiency only by the value of geometrical parameters: in Fig. 4 we call δ the misalignment, r is the coherence radius at the detection plane and L the linear size of a detection region. Under conditions $L > 2r$ and $\delta \ll L$, different types of mode are related to the measurable parameters as

$$\mathcal{M}_u = 2L\delta/\pi r^2 \quad (61)$$

$$\mathcal{M}_c = [(L - 2r)^2 - 2L\delta]/\pi r^2 \quad (62)$$

$$\mathcal{M}_b = 2L/r \quad (63)$$

By introducing the dimensionless parameters $X = L/2r$ and $D = \delta/2r$, the collection efficiency becomes

$$A = \frac{X(\pi\beta^2 - 2D(\mu + 1) - 2) + X^2 + 1}{X^2 + (\pi\beta - 2)X + 1} \quad (64)$$

Thus, in the limit $\mu \rightarrow 0$, the measured noise reduction factor in Eq. 59 does not depend on the mean number of photons. In the asymptotic limit $X \gg 1$, i.e. when the detection size is much larger than the correlation area, A and σ approach the unity and $1 - \eta$ respectively.

5. Sub-Shot-Noise absorption Imaging

Absorption imaging is one of the most popular and diffused imaging technique, used in many branches of science, especially in microscopy for biology. It is recognized from the biologist that the lowest photon dose should be used to probe and investigate biological

processes [100], where bright illumination can affect the regular biochemistry pathway or induce photo toxicity and damage [8]. Wide field absorption microscopy, is the simplest, fastest, less expensive and oldest imaging modality used, for example, for live-cell imaging. It has the advantage of requiring the lowest photon dose, especially for absorbed light imaging. But at low level of illumination, where few hundred/thousands photons/pixel/frame are collected, the photon shot noise starts to be an issue for the image quality.

Sub shot noise (SSN) absorption measurement has been demonstrated in dated work [101] using SPDC source, and recently re-proposed with the help of modern and more efficient devices [102] and exploiting heralded single photon sources [102]. However, these works focus on the estimation of a single value of the absorption, because only two correlated modes are exploited in a differential imaging configuration, see Sec. 5.1. Sub shot noise wide field imaging (SSNWF), where the whole spatial structure of the absorption profile is reconstructed, requires the exploitation of many, namely thousands, pair-wise correlated spatial modes which must be efficiently detected separately by a matrix of pixels. Thus, multi-mode quantum correlations generated by SPDC described in last Sec. 4, represent a valid tool for reaching SSN sensitivity in each pixels of the image [103], [104]. This section will provide a detailed description of SSN absorption measurements, presenting the latest achievements in the field [45, 105].

5.1. Absorption measurement

In absorption imaging [102] the sample is illuminated by a probe state and its transmitted pattern is imaged by the pixels of a 2D matrix, e.g. a CCD camera. The uncertainty in the absorption coefficient α , estimated by the measurement of the photon number $\langle \hat{N} \rangle$ [106] is:

$$\Delta\alpha = \frac{\sqrt{\Delta^2 \langle \hat{N} \rangle}}{\left| \frac{\partial \langle N \rangle}{\partial \alpha} \right|}. \quad (65)$$

In the following we will consider the uncertainty $\Delta\alpha$ in two different measurement scheme, namely direct imaging and differential imaging.

The direct imaging scheme is represented in Fig. 5 (a). A single probe beam is addressed to the object and the transmitted part is collected by a detector.

According to Eq. (3), the mean photons of the outgoing beam is $\langle \hat{N} \rangle = (1 - \alpha)\langle \hat{n} \rangle$, where $\langle \hat{n} \rangle$ is the mean number of the detected photons, as it would be without the object, it accounts the other losses and the detection efficiency. Referring to Eq. (3) of Sec.2 and substituting transmittance, the variance of the outgoing beam is

$$\langle \Delta^2 \hat{N} \rangle = (1 - \alpha)^2 [\langle \Delta^2 \hat{n} \rangle - \langle \hat{n} \rangle] + (1 - \alpha)\langle \hat{n} \rangle \quad (66)$$

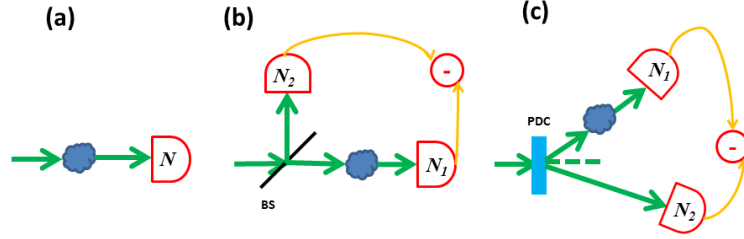


Figure 5. Simple sketch of the different imaging schemes. (a) Direct imaging. (b) Differential classical imaging, where classical correlated beams are generated by a balanced beam splitter. (c) Differential imaging with quantum correlated beams generated by SPDC.

Substituting Eq. (66) in Eq. (65), the uncertainty in the absorption estimation for the direct (DR) imaging scheme is

$$\Delta\alpha_{DR} = \sqrt{\frac{(1-\alpha)^2 [F-1] + (1-\alpha)}{\langle \hat{n} \rangle}}, \quad (67)$$

where F is the Fano factor defined in Sec. 3, as it would be measured in absence of the object. For a classical probe state ($F = 1$), the sensitivity scales as the usual shot noise limit, $\Delta\alpha_{DR} = \sqrt{(1-\alpha)/\langle \hat{n} \rangle}$. From Eq. (67) it is evident that a value of F smaller than the unit, representing non classical statistics of the probe state, allow surpassing the shot noise limit. However, as discussed in Sec. 3, Fano factor is deteriorated by the detection loss η . Thus, the non-classical behaviour in terms of noise reduction is lower bounded by $F_{det} = 1 - \eta$. It is important to note that splitting a single mode beam in \mathcal{N} pixels leads to a detection probability of the order of $\eta \leq 1/\mathcal{N}$ for each of them, ruling out the possibility of using a single mode for reaching sub-shot noise sensitivity. Even if sub-Poissonian light ($F < 1$) in single modes or few modes have been obtained, experimental complications in their generation and simultaneous detection limit their use for imaging, where higher number of non-classical spatial modes are needed, each mode addressing a single pixel. On the other side, as we have shown in Sec. 4, SPDC process produces naturally pair of beams, which are (individually) spatially incoherent (containing thousands of independent spatial modes) but are locally correlated in the photon number. Even if fluctuations of a single spatial mode in one beam are super-poissonian, due to photon number entanglement these fluctuations are perfectly replicated in the correlated mode of the second beam. This properties can be applied in a differential imaging scheme as described in the following.

Differential imaging exploits the correlation properties of two beams instead of one. These can be, for example, twin beams generated by SPDC as represented in Fig. 5(c), or a thermal beam split by a 50-50 BS, depicted in Fig. 5 (b). The scheme is the following: one of the two beams impinges on a absorbing object, with transmittance $(1-\alpha)$, before being detected. The other beam is directly detected, playing the role of reference for

the noise. Considering for simplicity the same losses on the two paths, the difference of mean photon numbers is proportional to the absorption coefficient:

$$\langle \hat{N}_- \rangle = \langle \hat{N}_2 - \hat{N}_1 \rangle = \alpha \langle \hat{n} \rangle \quad (68)$$

The variance in the photon number difference can be expressed in terms of the Fano factor and the NRF σ , defined in Eq. (12), in absence of the object as

$$\langle \Delta^2 \hat{N}_- \rangle = [\alpha^2(F - 1) + \alpha + 2\sigma(1 - \alpha)] \langle \hat{n} \rangle. \quad (69)$$

Therefore, the sensitivity in differential scheme can be evaluated according to Eq. (65), where here $N \rightarrow N_-$, as

$$\Delta\alpha_{DC} = \sqrt{\frac{\alpha^2(F - 1) + \alpha + 2\sigma(1 - \alpha)}{\langle \hat{n} \rangle}}. \quad (70)$$

The expression of the classical differential scheme can be obtained from Eq. (70) by substituting $\sigma = 1$. For a weakly absorbing object, $\alpha \rightarrow 0$, the term $\alpha^2(F - 1)$ is very small even for the super-Poissonian source and can be neglected. Thus, the uncertainty in the differential classical scheme becomes $\Delta\alpha_{DC} = \sqrt{(2 - \alpha)/\langle \hat{n} \rangle}$, which is a factor of $\sqrt{2}$ larger than the direct imaging for small α . The improvement provided by the quantum correlations ($\sigma < 1$) with respect to both the direct and the classical differential imaging can be evaluated by using Eq. (67) and Eq. (70) as

$$\begin{aligned} \frac{\Delta\alpha_{SSN}}{\Delta\alpha_{DC}} &= \frac{SNR_{SSN}}{SNR_{DC}} = \sqrt{\frac{\alpha + 2\sigma(1 - \alpha)}{2 - \alpha}} \approx \sqrt{\sigma} \\ \frac{\Delta\alpha_{DR}}{\Delta\alpha_{SSN}} &= \frac{SNR_{SSN}}{SNR_{DR}} = \sqrt{\frac{\alpha + 2\sigma(1 - \alpha)}{1 - \alpha}} \approx \sqrt{2\sigma}. \end{aligned} \quad (71)$$

Here, we have introduced the signal to noise ration, $SNR = \alpha/\Delta\alpha$, as a further figure of merit of the measurement sensitivity. From Eq. (71), it is clear that the advantage of quantum correlation can be quantified by the value of the non-classical parameter σ , which for twin beam is lower bounded only by the loss factor $\sigma = 1 - \eta$ (see Sec. 4.3). In particular the SSN condition, $\sigma < 1$, guaranties an advantage with respect to the differential classical scheme, while a more restrictive condition, $\sigma < 1/2$, is needed for the SSN scheme to beat the direct (shot-noise limited) one. This condition corresponds to the requirement of an overall loss in the detection of correlated photons smaller than 50%.

Actually one of the difficulties of the technique, when addressed to SSNWFI is to achieve a good collection efficiency of the correlated modes in the far field without sacrificing the spatial resolution. This is due to the trade-off between the collection efficiency and the pixel size as discussed in Sec. 4.4.

5.2. SSNWFI: experimental results

The first experimental demonstration of the SSNWFI involving many spatial modes has been given in 2010 Ref. [105]. Fig.6 presents the advantage of the quantum correlations

over direct and differential classical scheme. The weak absorbing π shaped object is hidden in the noise for both the classical imaging techniques, whereas its shape can be clearly identified in the image obtained using the SSN schemes of Fig. 5(c).

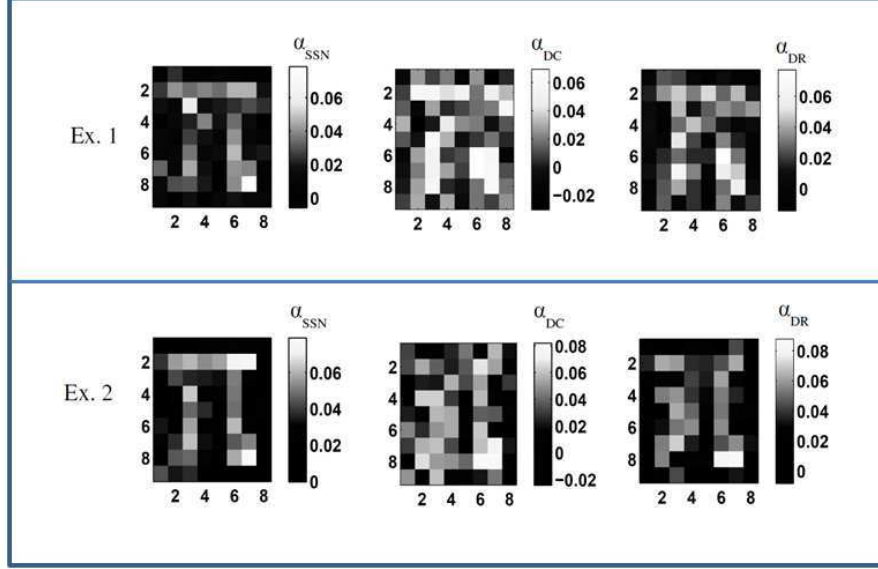


Figure 6. Two sets of typical images taken from the experiment in Ref. [105] are shown: SSN image (left), obtained by subtracting the quantum correlated noise; differential classical image (middle); direct classical image (right). The pixel size is $480 \mu m^2$, obtained by hardware binning of the physical pixels of the CCD to fulfill the condition $L > 2r$. For both sets of images the mean number of photons per pixel is $\langle \hat{N} \rangle \approx 7000$

It is important to mention that in this situation the image was obtained without any imaging lenses, basically revealing the shadow of the object placed closed to the detection plane. Thus, the resolution was not enough for any potential application in real world, especially in microscopy, where the technique would be naturally addressed. Moreover, the average NRF achieved $\sigma \simeq 0.5$ was not sufficient for beating the direct imaging in realistic condition on average, but only in a subset of the images acquired.

Very recently, an important step has been done with the realization of SSNWFI in a real microscopic configuration [45]. A noise reduction such as $\sigma = 0.8$ has been obtained for each pixel in a matrix of approximately 8000 pixels, and a spatial resolution of $5 \mu m$ at the sample. This noise reduction is enough to beat differential classical imaging, and the resolution is sufficient for the imaging of complex structures, like cells. Reducing the resolution of one third, allows to easily overcome the performance of the direct imaging scheme. The trade-off between the noise reduction and the resolution, according to the model of the collection efficiency developed in Sec. 4.4, is reported in Fig. 7 together with the improvement in the SNR with respect to both differential and direct shot noise limited classical imaging. The main difficulties with respect to classical microscopy are that the imaging systems should be able to reduce the aberration without introducing any losses. Fig.8 shows the experimental image profile of the sample (a “ ϕ ”-shaped few

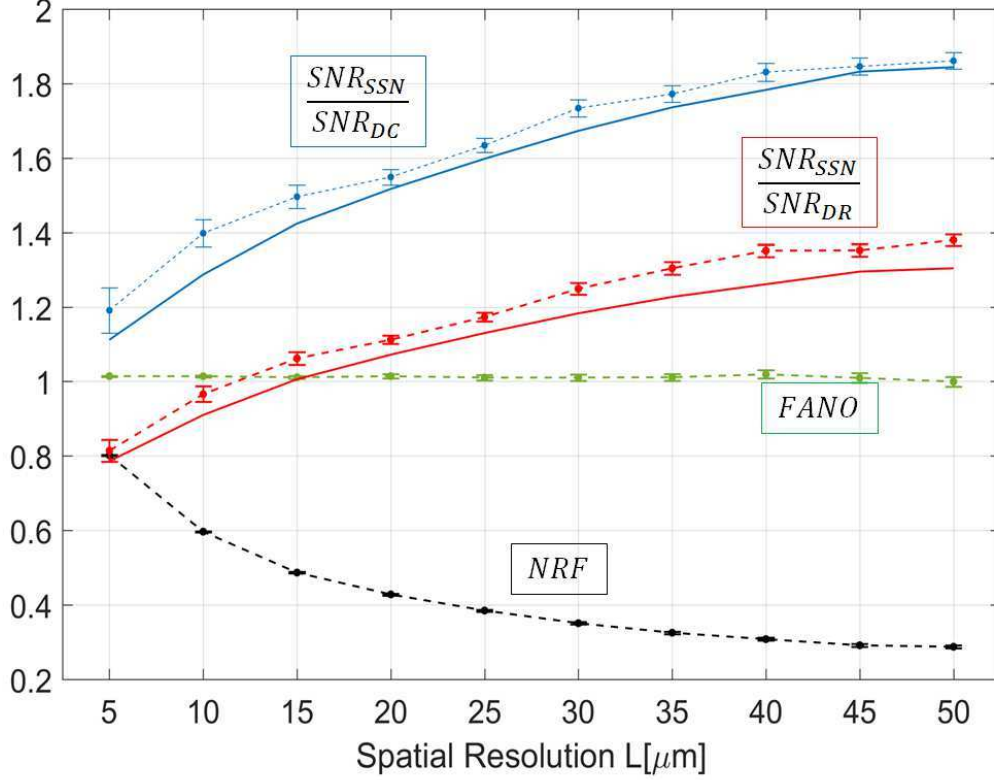


Figure 7. Experimental noise reduction factor (NRF) and signal-to-noise ratio (SNR) in function of the resolution in the focal (object) plane L . Black dots represents the NRF. The red dots are the SNR of the sub-shot-noise images normalized to the one of the direct images. For $L \geq 15\mu\text{m}$ there is the advantage of the quantum protocol. Analogously, the blue series shows that advantage of the sub-shot-noise imaging with respect to the differential classical imaging is present at any spatial resolution and reaches values of more than 80%. Solid lines correspond to the quantum enhancement predicted by Eq.s (71), when the estimated values of the NRF are considered.

nanometer thick deposition with absorption coefficient $\alpha = 1\%$) at different resolution scale L , so that $L = d \cdot 5\mu\text{m}$. From $d = 3$ the object start to appear in the SSN image, while remains almost undefined in the classical images.

Finally, we mention that differently from previous proof of principles of quantum enhanced phase-contrast microscopy exploiting NOON states ($N=2$)[19, 20, 21, 22], the SSN wide field microscope can offer the possibility of dynamic imaging without scanning the whole sample.

6. Target Detection in Preponderant Noise

The main stream of quantum enhanced measurement protocols focuses on the reduction of the uncertainty below shot noise limit (or standard quantum limit) which stems from the intrinsic quantum fluctuation of the probe beam itself and scales as $(n)^{-1/2}$, with n mean photon number of the beam. In this context it is recognized that

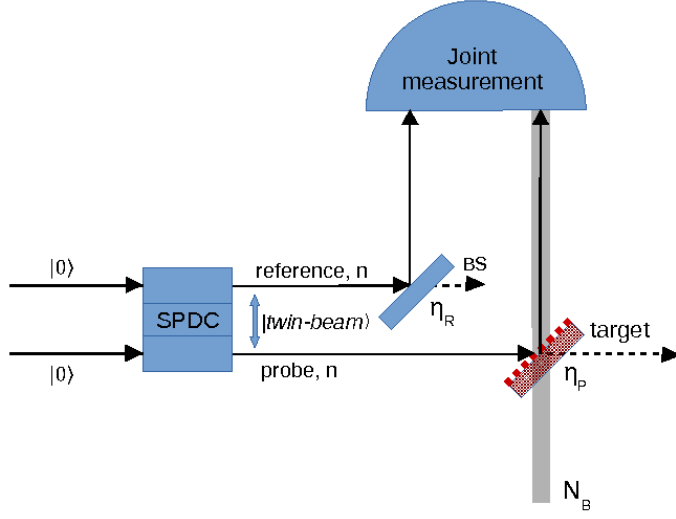


Figure 9. Scheme of the quantum illumination protocol proposed in [108], whose aim is to establish the presence of a target. One beam of the twin-beam is used as a reference, while the other, dubbed as probe, eventually interacts with the target. The reflected part of the probe mixes with a strong thermal background and goes to a detector, where also the reference beam is collected and a joint measurement is performed. η_R models losses on the reference path.

The optimal classical illumination is known to be product of \mathcal{K} identical coherent states $|\alpha\rangle$ and a homodyne-detection receiver [108, 111]. Homodyne detection measures the quadratures of the incoming field, in particular $\hat{x} = (\hat{a} + \hat{a}^\dagger)/2$. In this case $\langle \hat{x} \rangle = \langle \hat{x}_P \rangle + \langle \hat{x}_B \rangle$, where $\langle \hat{x}_P \rangle = \sqrt{\eta_P n}$ ($n = |\alpha|^2$) is the quadrature of the coherent probe after the object interaction and $\langle \hat{x}_B \rangle = 0$ is the quadrature of the thermal noise, which has zero-mean value. In the limit $n_B \gg n$ the noise of the measurement is dominated by the noise on $\langle \hat{x}_B \rangle$, equal to $\langle \hat{x}_B^2 \rangle = (2n_B + 1)/4$. The signal to noise ratio in the discrimination of the object presence is therefore:

$$SNR_{coh} = \sqrt{\frac{\mathcal{K}\eta_P n}{2\langle \delta^2 \hat{x}_B \rangle}} = \sqrt{\frac{\mathcal{K}\eta_P n}{n_B + 1}}$$

As mentioned, entanglement, in particular multi-mode SPDC state (see for example Eq. (35)), provides an advantage of 4 times in the exponent of the error probability, which is proportional to SNR [112]. The structure of the optimal 6dB-enhancement receiver is not known, however sub-optimal receivers with 3dB advantage has been already proposed and realized. They are based on non linear interferometer, i.e. a phase sensitive low-gain ($G - 1 \gg 1$) optical parametric amplifier (OPA). The idea is that the OPA output depends on the phase relation between the returning probe and the reference beam, while a completely dephased thermal beam does not. This

has enabled the experimental demonstration of the advantage of quantum illumination both in detection of a low reflection phase object [112] (a shift of the probe phase of 0 (π) correspond to the $H_1(H_0)$ hypotheses respectively), and for defeating passive eavesdropping attack in quantum communication [114, 113]. In particular the difference between the output signal in the two cases is proportional to the so-called phase sensitive cross correlation $\langle \hat{a}_1 \hat{a}_2 \rangle$ between the signal and idler field, which for two-mode squeezed state is $\sqrt{n(n+1)}$ largely exceeding the classical limit of correlation for a source with the same mean photon number n , in the limit $n \ll 1$. Recently a remarkable microwave/optical QI experiment has been reported as well [115]. Two elettro-optomechanical converters are used to entangle a microwave signal which is sent to the target region and an optical field retained at the source. The microwave radiation reflected by the target is then phase conjugated and upconverted into a second optical field that is jointly-detected with the retained one.

Both the quantum sub-optimal and classical optimal receiver described before are phase-sensitive measurement, requiring the probe to arrive at the receiver with a precise, unperturbed phase relation with a local oscillator or/and the reference beam. This could be not practicable in many context, also because it requires a precise mode matching at the receiver. Moreover, a quantum memory is needed, for example realized by an adjustable optical delay line (difficult to do if the distance of the object is not known a priori), to store the reference beam meanwhile the probe is propagating forth and back from the target object.

On the other side, in Ref. [116, 117] it has been proposed a version of quantum illumination considering a restricted scenario in which only intensity measurements (phase-insensitive) are exploited. The scheme is the one of Fig. 10. Here a photon number measurement is performed independently in the reference arm and in the probe arm, then the covariance of the two quantities is evaluated. Another difference with respect to the scheme of Ref. [108] is that the background field is not necessarily mixed to a beam splitter with the probe but more realistically reaches independently the detector. Note that in this specific framework, even the classical benchmark is different, with respect to the optimal one obtained in the more general context using homodyne detection. Similarly the quantum strategy cannot aim at achieving the optimal bounds of Ref. [108]. However, also in the contest where only intensity measurements are allowed, the quantum protocol maintains most of the appealing features of the original idea, like a huge quantum enhancement under similar conditions, $n \ll 1$ and $n_B \gg 1$, and a robustness against noise and losses. Moreover, even in this case, the advantage surprisingly survives when the quantumness at the detection state is broken. As we will show in detail in the next section, the SNR improvement provided by exploitation of quantum correlation in SPDC state with respect to the classical benchmark of a direct measurement of the mean photon number of a the returned probe is η_R/\sqrt{n} , where η_R represents here the losses on the reference channel. Moreover, introducing a further limitation, which is that a measurement of the background alone is not possible, i.e. the background and the reflected probe always come together at the receiver, the

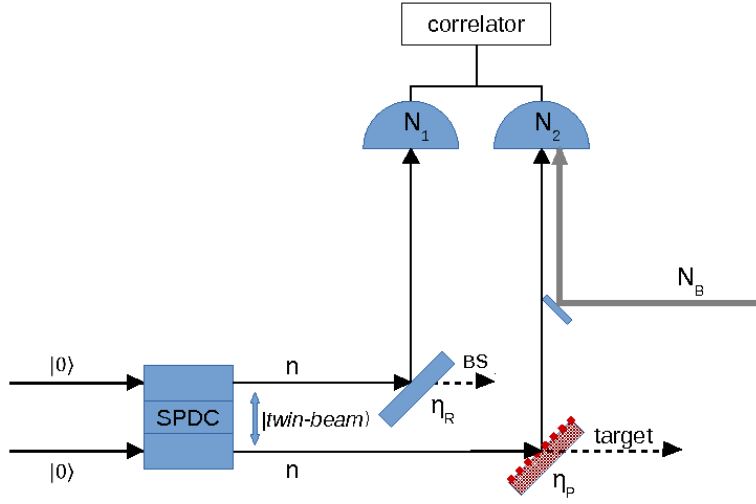


Figure 10. Scheme of the quantum illumination protocol proposed in [116], where only intensity measurements are performed. As in Fig. 9 one beam of the twin-beam is used as reference, while the other is the probe and interact with the target if it is present. The beams are collected by two detectors: n_1 is the number of the n photons of the reference beam which arrive at the first detector, n_2 is the sum of the photons eventually reflected from the target and the photons from the thermal back-ground, n_B . Note that we work in the approximation of $n_B \gg n$.

best classical strategy cannot be the direct measurement while is arguably the use of classical correlations. In this case the quantum advantage scales as $M/n = 1/\mu$, where M is the number of identical modes collected in the single measurement and μ is the mean number of spatial modes. Interestingly, this corresponds to the ratio of the total mutual information of classical and quantum correlated states [118].

In the spirit of this review, which explores the non-classical photon number correlation and their application in quantum enhanced measurement, in the next section we will describe in detail this last realization of the quantum illumination like protocol based on photon number correlation measurement.

6.1. Intensity correlation based QI

Let us consider first the direct scheme in which a probe with mean photon number n is addressed to the object and its reflected (transmitted) part reaches a detector together with a much stronger background with mean photon number n_B . Note that in this case only one beam is used. In the hypothesis H_0 only the background reaches the detector and the measured photon number is n_B , while for H_1 one has $\eta_P n + n_B$, their difference being the signal. The variance of the measurement is assumed to be dominated in both cases by the background fluctuations $\langle \delta^2 \hat{n}_B \rangle$. Thus, the signal to noise ratio obtained

by \mathcal{K} measurements is:

$$SNR_{Dr} = \frac{\sqrt{\mathcal{K}}\eta_P n}{\sqrt{2\langle\delta^2\hat{n}_B\rangle}} \quad (72)$$

Even if the strategy described above seems the most simple and natural approach, it assumes implicitly that it is possible to have an estimation of the mean photon number of the background itself: establishing a reference threshold of photocounts (the mean value of the background n_B) and comparing it with the value added with the mean photocounts coming from the reflected probe beam (if the target is present) it is possible to establish the presence of the object. If the background can not be measured separately, for example because the object is always present (of course this information is not available a priori), the previous method, simply based on the discrimination of two average intensity levels can not be applied. A second order measurement of the intensity is required instead, therefore we consider $\langle\delta\hat{n}_1\delta\hat{n}_2\rangle$, where $\delta\hat{n}_1$ and $\delta\hat{n}_2$ are the fluctuations on the reference and “probe+noise” beams respectively. The covariance $\langle\delta\hat{n}_1\delta\hat{n}_2\rangle_{H_0}$ in absence of the target is known to be null a priori, because the background and reference are uncorrelated, and establishes the natural zero-offset for the measurement. In presence of the target instead $\langle\delta\hat{n}_1\delta\hat{n}_2\rangle_{H_1}$ is in general different from zero and depends on the state used, i.e. on the correlations in photon number fluctuations between the two beams. In order to calculate the SNR it is necessary to consider also the uncertainty of the covariance. The fluctuation of this quantity is by definition, for $i = 0, 1$:

$$\langle\delta^2(\delta\hat{n}_1\delta\hat{n}_2)\rangle_{H_i} \equiv \langle(\delta\hat{n}_1\delta\hat{n}_2)^2\rangle_{H_i} - \langle\delta\hat{n}_1\delta\hat{n}_2\rangle_{H_i}^2. \quad (73)$$

As before if we consider the fluctuation in n_2 dominated by the background, both in presence and in absence of the target, i.e. $\delta n_2|_{H_1} \approx \delta n_2|_{H_0} = \delta n_B$, easy follows $\langle\delta^2(\delta\hat{n}_1\delta\hat{n}_2)\rangle = \langle\delta^2\hat{n}_1\rangle\langle\delta^2\hat{n}_B\rangle$. To evaluate SNR it is now necessary to explicit the state of light used. As said quantum illumination (QI) exploits the quantum correlation in photon number fluctuations of twin-beam state. In this case it holds, according to Sec. 4.3, $\langle\delta\hat{n}_1\delta\hat{n}_2\rangle_{H(1)} = n\eta_P\eta_R(1 + n/M)$, where M is the number of modes. Since each beam of this state is thermal for the single beam holds the multithermal (with M modes) statistics: $\langle\delta^2\hat{n}_1\rangle = n\eta_R(1 + \eta_R n/M)$. The SNR can be evaluated as:

$$SNR_{SPDC} \approx \frac{\sqrt{\mathcal{K}}\langle\delta\hat{n}_1\delta\hat{n}_2\rangle_{H_1}}{\sqrt{2\langle\delta^2\hat{n}_1\rangle\langle\delta^2\hat{n}_B\rangle}} \quad (74)$$

$$\begin{aligned} &= \frac{\sqrt{\mathcal{K}}n\eta_P\eta_R(1 + n/M)}{\sqrt{2n\eta_R(1 + \eta_R n/M)\langle\delta^2\hat{n}_B\rangle}} \\ &\approx \frac{\sqrt{\mathcal{K}}\eta_R n\eta_P}{\sqrt{2\langle\delta^2\hat{n}_B\rangle}} \end{aligned} \quad (75)$$

where the last approximation holds for $n/M \ll 1$, i.e. when the mean photon number per mode $n/M = \mu$ is small. We can now compare this result with the SNR

obtained with the direct measurement of the probe mean photon number (when this is possible). It results an improvement from using the quantum correlated state as large as $SNR_{SPDC}/SNR_{Dr} = (\eta_R/n)^{1/2}$.

It is also interesting to evaluate the advantage of the quantum correlation with respect to the possible use of classically correlated states. First line of Eq. (74) shows that classical and quantum scheme with the same local statistics, only differ for the strength of the correlation, quantified by the covariance $\langle \delta \hat{n}_1 \delta \hat{n}_2 \rangle_{H(1)}$. According to the generalized Cauchy-Schwarz inequality presented in Sec. 3, the covariance for classical beams is bounded by $\varepsilon = \langle \delta \hat{n}_R \delta \hat{n}_P \rangle / (\langle : \delta^2 \hat{n}_R : \rangle \langle : \delta^2 \hat{n}_P : \rangle)^{1/2} \leq 1$. Split thermal beams saturate the inequality, $\varepsilon_{TH} = 1$, with $\langle \delta \hat{n}_R \delta \hat{n}_P \rangle_{TH} = \eta_R \eta_P n^2 / M$, thus representing the best classical strategy. On the other hand the SPDC quantum correlation provides $\varepsilon_{SPDC} = M/n + 1$ with $\langle \delta \hat{n}_R \delta \hat{n}_P \rangle_{SPDC} = \eta_P \eta_R n(1 + n/M)$. Therefore, the comparison of the SNR with classical and quantum correlation immediately gives:

$$\frac{SNR_{SPDC}}{SNR_{TH}} = \varepsilon_{SPDC} = \frac{M}{n} + 1 = \frac{1}{\mu} + 1 \quad (76)$$

It is evident a dramatic quantum enhancement for a photon number per mode $\mu = n/M \ll 1$. Note that, as anticipated, the enhancement does not depend on the background intensity and it is also immune to the losses.

Finally we would like to trace a connection between the QI using an OPA receiver of Ref. [112] and the intensity measurement based scenario described above, showing that they have the same non-classicality /entanglement breaking condition. Indeed for a zero-mean Gaussian distributed bipartite state, the moment-factoring theorem allows to write the photon number covariance in terms of the modulus of the phase sensitive cross-correlation (measured by the OPA receiver): $\langle \delta \hat{n}_1 \delta \hat{n}_2 \rangle = |\langle \hat{a}_1 \hat{a}_2 \rangle|^2$. On the other side the normal ordered variance for a gaussian mode can be written in terms of the mean photon number: $\langle : \delta^2 \hat{n}_j : \rangle = \langle \hat{a}_j^\dagger \hat{a}_j \rangle^2$. Therefore, the non-classicality breaking condition, represented in general by the violation of the Cauchy-Schwarz inequality, in the framework of Gaussian states coincides with the entanglement breaking condition $|\langle \hat{a}_1 \hat{a}_2 \rangle|^2 \leq \langle \hat{n}_1 \rangle \langle \hat{n}_2 \rangle$ reported in Ref. [112], valid for single mode detection. Substituting in the Cauchy-Schwarz inequality the explicit expression of the photon statistics at the detectors, in the general multimode case, the condition becomes:

$$\eta_P \eta_R n \left(1 + \frac{n}{M} \right) \leq \left[\eta_R^2 \frac{n^2}{M} \left(\eta_P^2 \frac{n^2}{M} + \frac{n_B^2}{M_B} \right) \right]^{1/2} \quad (77)$$

In the limit of $\mu = n/M \ll 1$ the condition simplifies as $n_B \geq \eta_P (M M_B)^{1/2}$. For example when single modes are detected $M = M_B = 1$, a mean number of background photons $n_B > 1$ is enough to destroy Gaussian entanglement and more in general non-classical photon statistics, nevertheless the enhancement in the SNR remains.

6.2. Experimental implementation of quantum illumination

The experimental setup used in Ref. [116] for the realization of the intensity-correlation based QI protocol is represented in Fig. 14a. Type II SPDC generates pairs of correlated

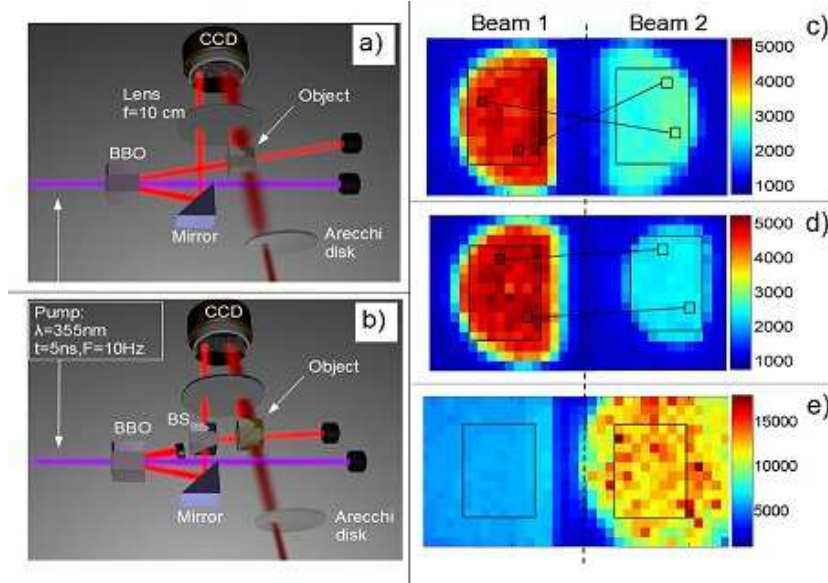


Figure 11. Experimental setup and examples of acquired frames. a) Quantum illumination (QI) b) Classical illumination (CI) c) Detected TWB, in the presence of the object, without thermal bath. The region of interest is selected by an interference filter centered around the degeneracy wavelength (710 nm) and bandwidth of 10 nm. After selection the filter is removed. d) Detected field for split thermal beams in the presence of the object, without thermal bath. e) A typical frame used for the measurement, where the interference filter has been removed and a strong thermal bath has been added on the object branch. The color scales on the right correspond to the number of photons per pixel.

5ns-pulses with average number of PDC photons per spatio-temporal mode $\mu \sim 0.1$, which are then addressed to a high quantum efficiency CCD camera. In the QI protocol (Fig. 14a) one beam (the reference) is directly detected, while a target object (a 50:50 BS) is posed on the path of the other one (the probe), where it is superimposed with a pseudo-thermal background produced by a laser beam scattered by an Arecchi's rotating ground glass. When the object is removed, only the background reaches the detector. The CCD camera detects, on different regions, both the optical paths. In the classical illumination (CI) protocol (Fig. 14b), the TWB are substituted with classical correlated beams, obtained by splitting a single arm of PDC, that is a multi-thermal beam, and by adjusting the pump intensity to ensure the same local statistics and spatial coherence properties for the quantum and the classical source.

n_1 and n_2 are the photon number detected by pairs of spatially correlated pixels in a single 5ns-shot of the pump laser, different examples of frames collected are reported in Fig. 14 c-d-e. Since many correlated pixels pairs are present, spatial statistics allow evaluating the covariance $\langle \delta \hat{n}_1 \delta \hat{n}_2 \rangle$ in a single shot, reducing the measurement time needed for asserting the presence or the absence of the target.

Fig. 12 reports the measured ε versus the theoretical prediction. One observes that for TWB ε_{QI} is in the quantum regime ($\varepsilon_{QI} > 1$) for small intensities of the thermal

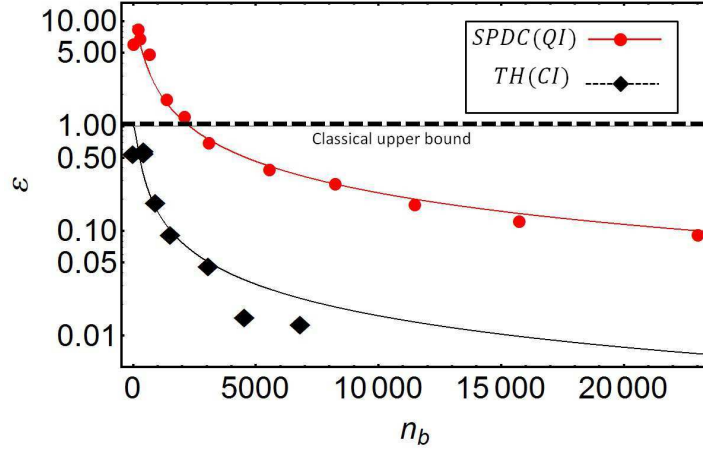


Figure 12. Generalized Cauchy-Schwarz parameter ε in the case of quantum illumination, ε_{QI} , and for the correlated thermal beams, ε_{TH} , as a function of the average number of background photons n_B (whith $M_B = 1300$). The lines represent the theoretical prediction for the estimated value of the mean photons number per mode $\mu = 0.075$.

background, reaching the value $\varepsilon_{QI} \simeq 10$ when $n_B = 0$. It rapidly decreases below the classical threshold according to the condition in Eq. (77) at the increasing of the background. For classical correlation of split thermal beams ε_{TH} is always in the classical regime, starting from $\varepsilon_{TH} = 1$ for $n_B = 0$, as expected.

In Fig. 13 an experimental comparison of the SNR for quantum and classical illumination is presented. While the SNR unavoidably decreases with the added noise for both QI and CI (see Eq. (74)), the ratio between them is constant regardless the value of n_B , in agreement with the theoretical prediction provided above, $SNR_{SPDC}/SNR_{TH} = \varepsilon_{SPDC} \simeq 10$. In turn, the measurement time, i.e., the number of repetitions \mathcal{K} needed for discriminating the presence/absence of the target, is dramatically reduced of 100 times when quantum correlations are exploited.

7. Ghost Imaging

Ghost imaging (GI) is an imaging technique theoretically proposed in 1994 [46] and experimentally realised in 1995 by Pittman et al. [47], using non classical states of light. Since then this technique has attracted great interest for the wide fields of its possible applications [119, 120, 121, 122, 123, 124, 125, 126, 127, 140].

The aim of this protocol is to retrieve the transmittance profile of an unknown object. To perform ghost-imaging two beams, whose intensity fluctuations are correlated, are necessary. The first beam, dubbed with 1, without interacting with the object, goes to a spatial resolving detector, i.e. a CCD camera. The second beam instead, dubbed here with 2, goes to the object we want to image and then to a bucket detector, e.g. a single-pixel photodetector. The procedure is repeated and \mathcal{K} frames

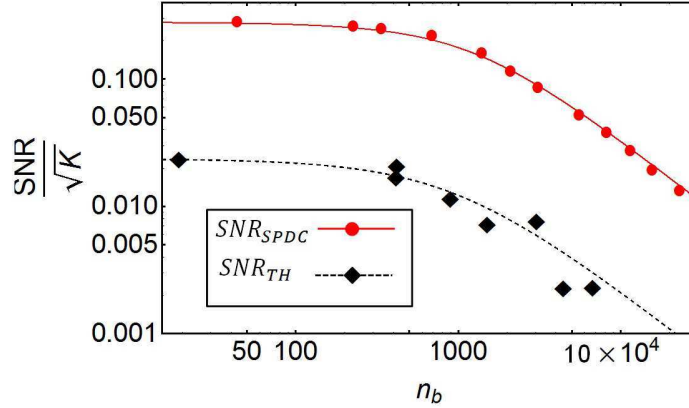


Figure 13. Signal-to-noise ratio (SNR) versus the number of background photons $\langle n_B \rangle$ normalized by the square root of number of realizations. The red (black) markers refer to quantum (classical) illumination. The curves corresponds to the theoretical model. Each experimental point is estimated by a statistics over a set of 6000 shots.

are collected. It is not possible to obtain the image of the object through signal from detector 1 or 2 separately, since the first one has not interacted with the object, while the other has no spatial resolution. Anyway, as we will see, correlating the signals from the two detectors it is possible to retrieve the image.

From this introductive description similarities between ghost imaging and quantum illumination performed using intensity measurement (described in Sec. 6.1) arise. Also comparing Fig. 10 and Fig. 14 the analogy is evident. In particular GI can be seen as a specific case of quantum illumination intensity protocol, where the background in the bucket-detector comes from the spatial modes of the source which are not correlated with the single pixel on the I -detector. Of course in GI the scanning of the I -arm allows a full spatial reconstruction of the object while in quantum illumination the goal is just to discriminate its presence in a specific point. Despite this difference, as discussed in the following, that the quantum enhancement in terms of signal-to-noise ratio assumes the same form both in quantum illumination and GI.

As it was in the first experimental realization of GI non-classical states of light, known as twin beams, can be used for this technique because of their perfect correlation in photon number. Nevertheless, it was shown, both theoretically and experimentally, that also beam-split thermal light can be used to perform GI, although with a smaller visibility ([128, 129, 130, 131, 132, 133]). In [134] is shown that even sunlight can be used, a result very interesting in view of future practical applications. These results started an intense debate and a lot of works were addressed to understand the differences between GI using classical (i.e. splitted thermal light) or quantum (i.e. twin-beam state) light and to establish the usefulness of quantum resources, in particular entanglement. To clarify the boundary between classical and quantum GI, different configurations were implemented and different measurements considered in order to find any evidence that

clearly distinguishes the two cases. An exhaustive discussion about the “quantumness” of GI is presented in [53], in this work competing interpretations of this technique are unified in a unique theoretical frame and misunderstandings about the role of entanglement are clarified. In particular it is shown the equivalence of the interpretation in terms of classical intensity-fluctuation correlations and two-photon interference both for pseudo-thermal or PDC light. From this argument it follows that experiments cannot distinguish between these two interpretations and therefore there is no measurement that cannot be reproduced both with classical or quantum light. The only difference between these two schemes is in terms of visibility, or better of signal-to-noise ratio (SNR). This is a consequence of the stronger correlations present in twin-beams. As we will see the, use of quantum light allows obtaining a better SNR and, in particular in low-illumination conditions, this enhancement becomes important. In this work we focus on this aspect presenting a simple theoretical model of GI, evaluating the SNR in quantum and classical case and discussing the quantum enhancement in different regimes.

Before going, in Sec. 7.1, into the details of GI technique let us review some of its possible applications and recent developments in order to appreciate how this technique offers important opportunities in a lot of different fields.

Since the image is retrieved from the *l*-beam, which does not interact with the sample, this method can be extremely useful in presence of phase distortions on the *2*-beam. This means that GI is particular interesting in presence of an object into a diffusive medium, condition that appears in several significant cases (as open air conditions or biological samples, where tissues represent the diffusive medium). Several works analysed performances of GI in turbid media, among the others [135, 136, 137]. Thanks to GI images can be retrieved much better than in standard noncorrelated direct imaging since it is insensitive to turbulence between the sample and the bucket detector while in [138] it is experimentally demonstrated that turbulence affects GI if it is between the source and the object and a theoretical model for a narrow sheet of turbulent air is presented. In the same article it is also proposed a possible solution in order to diminish the effect of turbulence slightly changing the GI apparatus. A concise but exhaustive theoretical treatment of turbulence and other aspects of non-ideality is also presented in [53].

In addition GI can be useful in particular experimental conditions, for example if the accessible volume in the proximity of the sample is limited: in this case the light beam interacting with the object can be collected simply with a single pixel detector as an optical fiber connected with a photodiode. This possibility is exploited for example in [139], where classical GI is applied to magneto optical imaging to perform Faraday microscopy. In this case the basic set-up is opportunely modified inserting a polarizer in front of the bucket detector. The initial polarization plane of the beam, interacting with the magnetized material and thanks to the Faraday effect, is rotated of an angle ϕ_{\pm} , whose sign depends on the magnetization sign: the polarizer has a different effect on the incident photon according to the magnetisation sign of the domain it crossed.

Exploiting this fact it is possible to retrieve the image of the magnetic domains in the sample.

In this work we will deal with GI conventional protocol, anyway several different variants have been proposed, both theoretically and experimentally. It is for example possible to retrieve the image of an object from reflected photons instead of the transmitted ones. This protocol has been experimentally realised in [140] and can offer interesting opportunities; in particular GI in reflection could find application as an alternative to the conventional laser radar for standoff sensing. To this aim in [141] the vulnerability of reflective GI to atmospheric turbulence is studied.

Another possible GI configuration is the so called “computational GI”. In the conventional GI with classical light the two beams are usually obtained sending a laser beam to a time-varying (rotating ground-glass) diffuser and then to a beam splitter. In [142] it was argued that the ground-glass diffuser can be replaced with a spatial light modulator (SLM). Applying deterministic modulation to the SLM and then correlating this signal, opportunely processed, to the output of the bucket detector is possible to retrieve the object. Notice that in this case only the bucket detector is used. Computational ghost imaging was experimentally implemented by Bromberg et al. [143]. The same authors further developed this technique introducing the compressive ghost imaging method [144], also used later in [141].

Different works, as for example [145, 146, 147], explored the possibility of the so called “two-wavelength GI”. Every two-detector case we have considered so far has assumed single-wavelength operation: it means that in the quantum case we were working around PDC frequency degeneracy while in the classical case this condition comes simply from using a laser and then a beam-splitter. Performing GI with beams at a significantly different wavelength can offer advantages: on one hand high spatial-resolving and/or efficient detectors are not available at all wavelengths, on the other atmospheric turbulence and scattering effects are sensitive to wavelength. Thus, using a downconversion source, whose beams match these different conditions, can yield to an improvement in the image quality.

To conclude, from the first idea of GI and its original protocol several applications to different fields and several extensions have been proposed. The ones described above are far from being exhaustive. For instance, the use of higher-order correlations to form ghost images has also been considered [148, 132] as has the use of homodyne detection instead of direct detection [149].

In the following we intend to focus on the quantum enhancement offered by twin-beams, discussing in which limits they provide an advantage respect to the classical light.

Since we will see that quantum enhancement is particularly important at low illumination level, before moving to the next section we conclude discussing a recent experiment working in this condition. In [150] the authors succeed in obtaining a high-quality image of an object using less than 0.5 photons per pixel. To achieve this amazing result GI protocol with quantum light was used. Anyway it was opportunely

adapted, both in the experimental apparatus and in data analysis, to work in this peculiar condition. The key idea of the experimental set-up is to use an Intensified CCD camera (ICCD) and to exploit the spatial correlation between the two entangled photons in *1* and *2*-arm triggering the intensifier of the ICCD with an external pulse from the bucket *2*-detector. In this way a photon is measured by the resolving *1*-detector only if its correlated one hits the bucket detector (i.e. if not absorbed). Using this time-gated imaging system the image can in principle be retrieved directly on the resolving detector. Experimentally, working at very low photon-flux, each frame contains only few photons, and therefore effects of Poissonian noise are not negligible and do not allow to distinguish the object. To obtain a great-quality image a reconstruction technique was used, in particular exploiting the natural sparsity in the spatial frequency domain of typical images and the Poissonian nature of the noise on the experimental data. This method was also tested on a biological sample; biological imaging could be one of the most important applications of imaging at low illumination level since in this case samples can be sensitive to high fluxes, developing new techniques in this direction is therefore of the utmost interest.

7.1. Theory of conventional GI

Let us move to describe in details how conventional GI technique works. A scheme of the experimental set-up is shown in figure 14. The image of the object is retrieved by

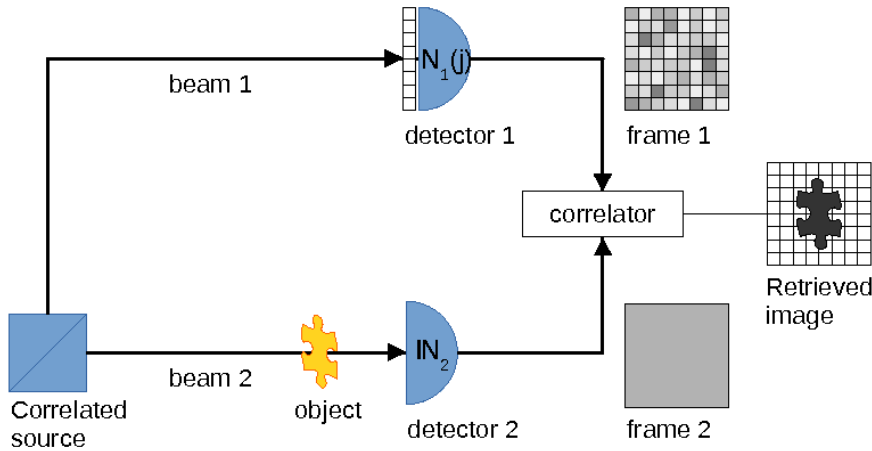


Figure 14. Ghost imaging schematic representation: two beams *1*-beam and *2*-beam, whose intensity fluctuations are correlated, are sent to two distinct optical path: one containing a spatial resolving detector *1*, and the other one containing the object to be imaged and a bucket detector *2*. The image of the sample is retrieved correlating the output of the two detectors.

measuring the function $S(x_j)$, where x_j is the position of the pixel j of the resolving detector, in arm *1*. In general $S(x_j)$ can be written as a function involving the correlation

functions at different orders of the output of the two detectors:

$$S(x_j) = f(E[\mathbb{N}_2], E[N_1(x_j)], E[\mathbb{N}_2 N_1(x_j)], \dots, E[\mathbb{N}_2^p N_1^q(x_j)]) \quad (78)$$

where $\mathbb{N}_2 = \sum_i N_2(x_i)$ is the total number of photons collected at the bucket detector 2 and $N_1(x_j)$ is the number of photons collected in the j pixel of the resolving detector 1.

Experimentally we evaluate these quantities averaging on the number of frames \mathcal{K} : $E[X] = \frac{1}{\mathcal{K}} \sum_{k=1}^{\mathcal{K}} X_k$.

The ghost image can be retrieved by exploiting different GI protocols, namely, different expressions for $S(x_j)$ [151]. In this work we focus on the covariance between the two output. Note that the covariance between the output from the two detector is exactly the quantity considered in quantum illumination.

$$\begin{aligned} S(x_j) &= \text{Cov}(\mathbb{N}_2, N_1(x_j)) \equiv E[\{\mathbb{N}_2 E[\mathbb{N}_2]\} \{N_1(x_j) E[N_1(x_j)]\}] \\ &= E[\mathbb{N}_2 N_1(x_j)] E[\mathbb{N}_2] E[N_1(x_j)] \end{aligned} \quad (79)$$

To quantify the quality of the image obtained and to compare quantum and classical GI we consider the signal-to-noise ratio (SNR). It is defined as:

$$SNR = \frac{|\langle S_{in} - S_{out} \rangle|}{\sqrt{\delta^2 S_{in} + \delta^2 S_{out}}} \quad (80)$$

where S_h , $h = in, out$ are the intensity values of the reconstructed ghost image, when x_j is respectively inside or outside the object profile. For the sake of simplicity we assume a uniform object of transmittance $T = T_{2-}$, while the transmittance outside the object is $T = T_{2+}$. $\delta S_h \equiv S_h - \langle S_h \rangle$ is the fluctuation of S around its average and $\delta^2 S_h$ is its variance. Finally, both the mean value, $\langle S_h \rangle$, and its variance $\delta^2 S_h$ can be experimentally estimated by performing space averages over the regions in and out. The theoretical values of these quantities, and therefore the theoretical value of SNR depend on which states of light are under consideration.

In the following we compare spatially incoherent, locally correlated thermal beams and twin-beam states. The first state is usually obtained by splitting a single pseudo-thermal beam through a beam-splitter. In this case it holds:

$$\langle \hat{N}(x_j) \rangle_{TH} = T(x_j) M \mu = T(x_j) \langle \hat{n}_j \rangle \quad (81)$$

$$\text{Var}(N(x_j))_{TH} = T(x_j) M \mu (1 + T(x_j) \mu) = \langle \hat{n}_j \rangle \left(1 + \frac{\langle \hat{n}_j \rangle}{M} \right) \quad (82)$$

where μ is the mean number of photons per mode, M is the number of modes detected by each pixel and $T(x_j)$ is the transmittance in correspondence of pixel j . For $M \gg \langle \hat{N}(x_j) \rangle$ we have $\text{Var}(N(x_j)) = N(x_j)$: in this limit thermal light can be described with a Poisson distribution.

As described in Sec. 4 the twin beam state is a quantum state of light that can be produced by the non-linear optical phenomenon of parametric down conversion and presents perfect correlation in photon number fluctuation. This perfect correlation is intrinsically quantum, nothing similar is possible for classical light. Anyway, since at

single mode level they present a thermal statistics Eq. (81) and Eq. (82) describe also the single beam of this state.

The difference between split classical-thermal-light and twin-beam state arises when considering the expressions for the covariance between photon number fluctuations in the two beams. In both cases the covariance is not null only considering correlated modes:

$$\langle \delta \hat{N}_2(x_i) \delta \hat{N}_1(x_j) \rangle_{TH} = T_2(x_i) T_1(x_j) M \mu^2 \delta_{i,j} \quad (83)$$

$$\langle \delta \hat{N}_2(x_i) \delta \hat{N}_1(x_j) \rangle_{SPDC} = T_2(x_i) T_1(x_j) M \mu (1 + \mu) \delta_{i,j} \quad (84)$$

The photon-number fluctuation correlation for thermal light is relevant when the number of photons per mode is $\mu \gg 1$, and therefore in this case it can be exploited to perform GI. Anyway, it does not include the shot-noise component $\propto \mu$, which remains uncorrelated [151]. From Eq. (84) it emerges that in twin-beams even the shot-noise component of the fluctuations is correlated: this is at the basis of quantum enhancement.

Before proceeding in the comparison we are interested in, we show how considering $S(x_j) = \text{Cov}(\mathbb{N}_2, N_1(x_j))$ it is possible to retrieve the object transmittance profile. We report the calculation for classical GI but the principle is the same also for quantum GI.

$$\begin{aligned} S(x_j)_{TH} &= \langle \delta \hat{N}_2 \delta \hat{N}_1(x_j) \rangle_{TH} \\ &= \sum_i \langle \delta \hat{N}_2(x_i) \delta \hat{N}_1(x_j) \rangle_{TH} \\ &= T_1(x_j) T_2(x_j) M \mu^2 = T_1 T_2(x_j) M \mu^2 \end{aligned} \quad (85)$$

where the last equivalence holds in the hypothesis of uniform transmittance on arm 1. From Eq. (85) we have that $S(x_j)$, the quantity experimentally measured, is proportional to the transmittance coefficient on arm 2 in the position x_j .

7.2. Comparison of classical and quantum case in terms of SNR

To compare GI performances in classical and quantum case SNR in the two situations is theoretically evaluated. For $\langle S_{in} \rangle_l$ and $\langle S_{out} \rangle_l$, $l = cl, q$, we use Eq. (83) and Eq. (84) for classical and quantum case respectively. Similarly as what has been done in quantum illumination in Eq. (73) the variance of these quantities, $\delta^2 S_{out}$ and $\delta^2 S_{in}$, is obtained by:

$$\delta^2 S_h(x_j) \equiv \frac{\langle (\delta \hat{N}_2 \delta \hat{N}_1(x_j))^2 \rangle - \langle \delta \hat{N}_2 \delta \hat{N}_1(x_j) \rangle^2}{\mathcal{K}} \simeq \frac{1}{\mathcal{K}} \langle \delta^2 \hat{N}_2 \rangle \langle \delta^2 \hat{N}_1(x_j) \rangle \quad (86)$$

by averaging over the region outside the object and the one inside to obtain $\delta^2 S_{out}$ and $\delta^2 S_{in}$ respectively. We define R_m the number of pixels corresponding to transmittance T_{2m} , $m = +, -$ (as said T_{2+} is the transmittance outside the object while T_{2-} is the transmittance inside). The first equality in Eq. (86) is simply the definition of variance, while the second one holds under the hypothesis of $R_m \gg 1$: in this case \mathbb{N}_2 and

$N_1(x_j)$, $x_j \in R_m$ can be considered independent since only one pixel over a great number of pixels in R_m is correlated. Considering Eq. (82) and that

$$\begin{aligned}\langle \delta \hat{N}_2 \rangle &= \sum_j \langle \delta^2 \hat{N}_2(x_j) \rangle = \\ &= \sum_{x_j \in S_{in}} \langle \delta^2 \hat{N}_2(x_j) \rangle + \sum_{x_j \in S_{out}} \langle \delta^2 N_2(x_j) \rangle = \\ &= R_- T_- M \mu (1 + T_- \mu) + R_+ T_+ M \mu (1 + T_+ \mu)\end{aligned}\quad (87)$$

we have:

$$\delta^2 S_h = \mathcal{K}^{-1} [R_- T_- M \mu (1 + T_- \mu) + R_+ T_+ M \mu (1 + T_+ \mu)] T_1 M \mu (1 + T_1 \mu) \quad (88)$$

It is important to notice that this expression is the same both in thermal or quantum case: this comes from the fact that the single beam of a twin-beam state is thermal.

From the definition of SNR (Eq. (80)), replacing formulas and rearranging terms:

$$SNR_{TH} = \sqrt{\mathcal{K}} \frac{\sqrt{T_1} \mu (T_{2+} - T_{2-})}{\sqrt{2(1 + T_1 \mu) [R_- T_- (1 + T_- \mu) + T_{2+} R_+ (1 + T_{2+} \mu)]}} \quad (89)$$

$$SNR_{SPDC} = \sqrt{\mathcal{K}} \frac{\sqrt{T_1} (1 + \mu) (T_{2+} - T_{2-})}{\sqrt{2(1 + T_1 \mu) [R_- T_- (1 + T_- \mu) + T_{2+} R_+ (1 + T_{2+} \mu)]}} \quad (90)$$

As expected the SNR increases with \mathcal{K} , number of frames collected, while the dependence on other parameters is more complex. To understand these expressions, physically interesting limits are considered in the following.

- We firstly consider the case of $\mu \gg 1$, which is the situation of high number of photons per modes. In order to further simplify the expressions we also consider the case of $T_{2+} = 1$ and $T_{2-} = 0$ (the detector detects all and only the photons that do not hit the object, modeled as perfectly absorbing).

$$\mu \gg 1 : SNR_{TH} = SNR_{SPDC} = \sqrt{\mathcal{K}} \frac{T_{2+} - T_{2-}}{\sqrt{2} \sqrt{T_{2+}^2 R_+ + T_{2-}^2 R_-}} \quad (91)$$

$$T_{2+} = 1; T_{2-} = 0 : SNR_{TH} = SNR_{SPDC} = \frac{\sqrt{\mathcal{K}}}{\sqrt{2R_+}} \quad (92)$$

In this limit the same expressions are found both in classical or quantum case. This result is not surprising and comes from the fact that for $\mu \gg 1$ the expressions for the covariances converges to the same value. Looking at Eq. (91) it results that in this limit the SNR does not depend on T_1 , that is the transmittance on channel 1.

- In the opposite case, for $\mu \ll 1$, the expressions become:

$$\mu \ll 1 : SNR_{TH} = \sqrt{\mathcal{K}} \frac{\sqrt{T_1} (T_{2+} - T_{2-})}{\sqrt{2[R_- T_{2-} + T_{2+} R_+]}} \mu \longrightarrow 0 \quad (93)$$

$$SNR_{SPDC} = \sqrt{\mathcal{K}} \frac{\sqrt{T_1} (T_{2+} - T_{2-})}{\sqrt{2[R_- T_{2-} + T_{2+} R_+]}} \quad (94)$$

$$\text{for } T_{2+} = 1 \text{ and } T_{2-} = 0 : SNR_{SPDC} = \frac{\sqrt{\mathcal{K}}\sqrt{T_1}}{\sqrt{2R_+}} \quad (95)$$

In this limit the difference between the two cases is evident: while in the classical case the SNR decreases proportionally with μ and approaches 0 as soon as $\mu \rightarrow 0$, in the quantum case the SNR converges to a constant value. It is important to notice that this constant depends on \mathcal{K} , and can therefore be arbitrary increased with a longer acquisition time experiment.

Moreover, in both regimes considering $T_{2+} = 1$ and $T_{2-} = 0$, $SNR \propto \frac{1}{\sqrt{R_+}}$. For a fixed total area, having a great R_+ means having a little R_- , that is considering a little object: this result therefore reproduces the reasonable fact that it is more difficult to image a little object. We also recall that all these expressions for SNR are obtained in the limit $R_+ \gg 1$, necessary hypothesis to consider N_2 and N_1 independent.

To conclude the comparison of classical and quantum ghost imaging and discuss the quantum enhancement we can consider the ratio of the two SNRs, G . From the exact expressions in Eq. (89) and Eq. (90):

$$G = \frac{SNR_{SPDC}}{SNR_{TH}} = \frac{1}{\mu} + 1 \quad (96)$$

The only dependence is on μ : to quantify the quantum enhancement it is fundamental to consider the value of μ we are working at.

- For $\mu \gg 1$, $G \rightarrow 1$: in this regime, as it appears considering Eq. (91), the quantum and classical case are equivalent in terms of SNR. The quantum enhancement is in this case negligible.
- For $\mu \ll 1$, $G \rightarrow \infty$: this is the regime where the quantum enhancement is more important. Only using twin beam states it is possible to retrieve the object profile.

As we pointed out in the introduction the analogy between GI and quantum illumination is confirmed by Eq. (96) which is exactly the same as the one in Eq. (76).

In order to perform a probably more useful comparison in practical situations, we introduce the “illumination level”, defined as

$$I_d \equiv \langle \hat{N}_1 \rangle = T_1 M \mu \text{ or } I_{ob} = M \mu \quad (97)$$

I_d represents the total number of photons detected in a single pixel of the camera (T_1 being the detection efficiency). In presence of cameras with a low level of saturation this is the quantity of the greatest interest. I_{ob} , representing the total number of photons that hit the object in a surface corresponding to 1 pixel of the resolving camera, is the relevant quantity not to be exceeded when considering a damageable object.

In terms of these quantities Eq. (96) becomes:

$$G = \frac{SNR_{TH}}{SNR_{SPDC}} = \frac{I_d}{T_1 M + I_d} \quad \text{and} \quad G = \frac{I_{ob}}{M + I_{ob}} \quad (98)$$

Also from these expressions appears that the best quantum enhancement is in correspondence of low illumination level, while for high illumination level the two situations are almost equivalent. Finally, for a fixed illumination level, higher is the number of spatio-temporal modes M (or $M T_1$ if we consider I_d) higher is the quantum enhancement.

After a general presentation of ghost imaging technique and some of its possible applications and configurations we presented a simple model of GI in order to discuss the enhancement offered by quantum states of light. The model shows how exploiting correlations in photon number fluctuations it is possible to achieve the surprising result of imaging an object thanks to a beam, which does not interact with the object itself and another going to the object and then collected by a single-pixel detector. We particularised this model considering two different possible states of light: splitted thermal light and twin-beam state. Finally, we compare their performances in terms of SNR, both in the general case and in two interesting limits. In the discussion about the quantum enhancement μ , mean number of photons per spatio-temporal mode, plays a fundamental role. Its dependence in terms of illumination level, a quantity that can be experimentally more important, was also reported. When $\mu \gg 1$ the classical and quantum case are almost equivalent. Therefore, in this situation, considering the less demanding experimental resources, classical light is the best solution. In the opposite regime, when $\mu \ll 1$, the behaviour in the two cases is deeply different: in the classical case $SNR \rightarrow 0$ while in the quantum one it converges to a finite value. This result is of great interest since we can have experimental situations where μ must be very low not to damage the sample under analysis. This consideration paves the way for a lot of interesting applications of quantum ghost imaging in situations where a low light level is needed, as for example in the imaging of certain biological samples.

8. Detector Absolute Calibration

The exploitation of quantum correlations for measurements of losses finds a special application in the field of quantum radiometry [152]. Specifically, in this case, we are interested in the capability to estimate the quantum efficiency of a photon detector in an absolute way, i.e. without the use of pre-calibrated devices or reference standards.

Calibration techniques at the level of single or few photons are fundamental for several rising technologies that exploit quantum states of light, like quantum computation [153], quantum key distribution [154] and quantum imaging [13], in which it is mandatory to have well calibrated detectors.

The quantum efficiency η represent one of the most important figures of merit for photon detectors and it is defined in the most general case as the overall probability of detecting a single photon impinging on the detector.

$$\eta = \frac{(\text{Number of detected photons})}{(\text{Number of impinging photons})}. \quad (99)$$

In order to review the calibration techniques exploiting quantum correlation

developed in recent years, it is useful to divide the light detectors in two main categories: analogical detectors and single photon detectors. Analogical detectors provide a signal proportional to the radiant flux impinging on the sensor, usually they are not able to detect single photons due to the high noise level and are designed to work at medium/high light intensity. Otherwise, single photon detectors have a resolution that allows discriminating single photons, but usually they are limited to working at low light intensity due to saturation effects. We can also divide the single photon detectors in click/no-click detectors and Photon Number Resolving (PNR) detectors. The firsts can only discriminate between zero photons detected (no-click) and one or more photons detected (click) in a time window depending by the detector characteristics. Otherwise, PNR detectors are able to provide the number of impinging photons also if they arrive simultaneously.

It is important to note that, currently, at single/few photons level there are no absolute detectors (detector with predictable quantum efficiency) or standard references (deterministic single photon sources) that have a stability and an accuracy suitable for metrological purposes. Therefore, absolute techniques based on quantum correlations are an important tool for providing calibrated single photon detectors suited for the mentioned technologies and represent a valid alternative to the classical calibration approach to the efficiency estimation. Such techniques exploit intense calibrated sources and calibrated attenuators to provide well-known and controlled input states. We also mention that, modern quantum tomographic methods allows to numerically reconstruct, not only the quantum efficiency, but also the whole positive operator-valued measure (POVM) of the detector [157, 158, 159, 160, 161, 162, 163, 164, 165].

Some alternative techniques for absolute calibration has been demonstrated recently, based on squeezed light [155] and on coherent states [156].

Furthermore, detectors are not the only elements of quantum technologies that need an accurate calibration. For example, in many quantum communication implementations, it is necessary to have a full characterization of the quantum channel. Also in this case quantum correlations are an important tool [166] for the characterization protocols.

8.1. Klyshko's method for absolute calibration of single photon detectors

The first calibration method exploiting quantum correlations was proposed in the seventies of twentieth century by Klyshko [167, 168], but only in the nineties the technological development allowed performing experimental demonstrations of accurate calibrations [169]. Nowadays, Klyshko's calibration technique is recognised as a fundamental metrological tool by the international radiometric community [170, 171, 172, 50, 173, 174, 175, 176].

The Klyshko's method is based SPDC described in Sec.4.

Because photons emitted by SPDC are always produced in pairs, with strong time correlation, the presence of a number n of photons, in a particular optical mode,

guarantees the presence of n photons in the conjugate optical mode. Traditionally, the two conjugated optical modes are called signal and idler and we refer to them with the subscripts s and i respectively.

In the basilar Klyshko's technique are used two click/no-click single photon detectors. The first is the Device Under Test (DUT) of which we want to determine the quantum efficiency η_1 and this is used to detect photons on the idler path. The second is the trigger detector. Also this has an unknown quantum efficiency η_2 and it is used to detect photons on the signal path, as shown in Fig. 15.

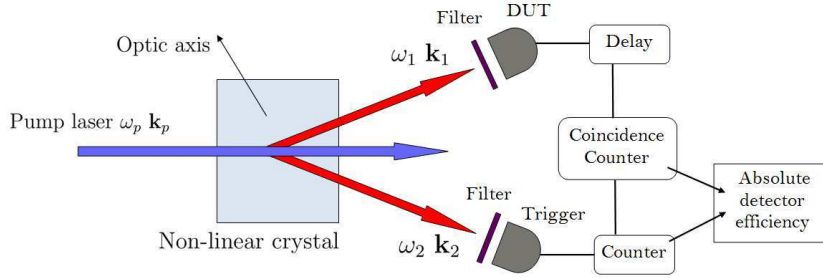


Figure 15. Scheme of a typical apparatus for Klyshko's calibration technique

If the total number of emitted pairs is n , then the number of photons detected by the idler detector is $n_1 = \eta_1 n$, whereas the number of photons observed by the signal detector is $n_2 = \eta_2 n$. Detectors output signals are addressed to a timing electronics counting the number of coincidences that occurs in a determined interval. A coincidence occurs when two photons are detected simultaneously, within a certain window, in both the detectors. The number of coincidences is given by $C = \eta_1 \eta_2 n$. This expression is the analogue of the covariance in Eq. (50) in the limit of low gain in which the mean number of photon per mode is very small ($\mu \rightarrow 0$).

Assuming that there are not external losses on the optical paths and assuming to have detectors that are not affected by noise, it is possible to determine the efficiency η_1 simply by taking the ratio $\eta_1 = C/n_2 = (\eta_1 \eta_2 n)/(\eta_2 n)$.

When real devices are used, this simple formula has to be modified to account for the presence of noise and losses. First, we have to consider that in addition to the desirable correlated photons, each detector has a number n_b of background counts, consisting of unwanted external light, dark counts due to thermal noise and electronic noise. The true number of desirable photons n_t is then the measured number of photons n_m minus the background B (determined in a separate measurement in which the SPDC emission is interdicted). Second, we have to consider spurious coincidence counts caused by the finite duration w of the coincidence window. The true number of coincidences C_t is then given by $C_t = C_m - A$ where C_m is the measured value and A the accidental coincidences.

For losses, we can identify two kinds of contributions: losses due to optical elements of the DUT detector and losses in the path from the core of the SPDC crystal to the detector.

For what concerns losses due to optical elements of the detector, we have to consider the overall quantum efficiency of the detector including lenses, filters and apertures. Therefore η is not only the quantum efficiency of the sensitive region of the detector, but includes also this kind of losses.

Concerning path losses, it is necessary performing an independent estimation of the path transmissivity γ and, if they are substantial, we have to take into account this contribution. In most of practical cases $\gamma \approx 1$.

Combining these effects, it is possible to calculate the DUT detector efficiency in terms of other measurable quantities:

$$\eta_1 = \frac{C_m - A}{\gamma(n_2 - B)} \quad (100)$$

The only way to know the internal quantum efficiency η_{int} is to calibrate independently the overall transmissivity γ of all optical elements of the detector and divide the whole quantum efficiency for that quantity: $\eta_{int} = \eta/\tau$.

Notice that the efficiency of the idler detector does not appear in Eq.(100), this confirms that Klyshko's calibration technique is absolute and no pre-calibrated references are needed.

It is important to note that, due to the inability of the involved detectors to discriminate more than one photon, it is necessary to set the parameters of SPDC process in order to have a negligible probability to emit more than one couple of photons in the detection time window of the detectors.

Recently, many variants and improvements of the Klyshko's technique have been studied. The most important of these are the methods to calibrate PNR detectors and CCDs that will be detailed in the next sections of this chapter. In addition, others techniques merit mention, like: the single-photon detector calibration based on conditional polarization rotation [177].

8.2. Extension of Klyshko method for PNR detector calibration

Photon number resolving detectors are an important tool in many fields of science and technology [178, 179]. Photon number resolution can be achieved by multiplexing click/no-click detectors [180, 181, 182, 183] or using intrinsically PNR detectors like photo-multipliers [184, 185, 186, 187], visible light photon counters [188, 189], transition edge sensors (TESs) [190] and Inductive Superconducting Transition Edge Detectors (ISTEDs) [191].

Of course, the basic version of the Klyshko's technique can be used to calibrate PNR detectors. However, a direct application of such method does not exploit the full potential of a PNR detector because it does not take into account the possibility to have more photons simultaneously. An extension of the Klyshko's method that involves contribution of one or more photons couples at a time has been developed recently [192].

The apparatus, shown in Fig.16, is equivalent to the previous one, with the only differences that, now, the DUT is a PNR detector and the intensity of SPDC emission

is enough to have a non-negligible probability to produce more than one photon in the detection time window. The trigger detector on the idler beam is still a click/no-click detector with unknown quantum efficiency.

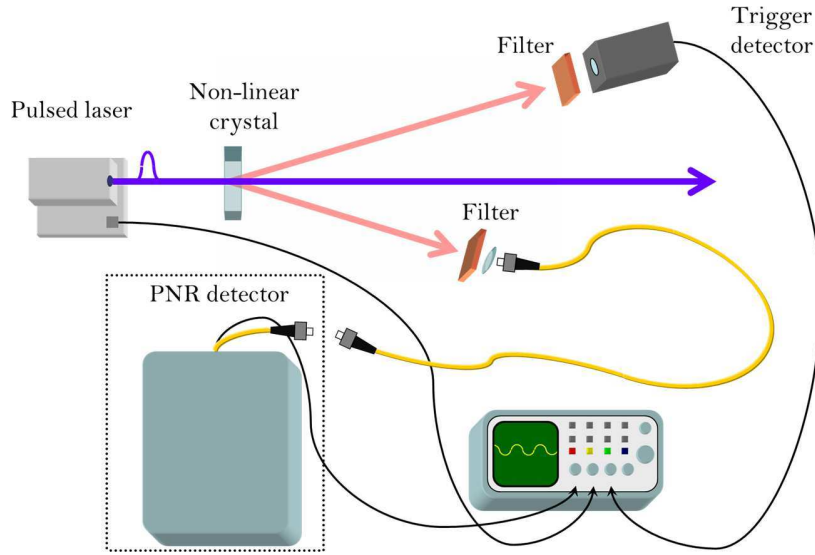


Figure 16. Experimental scheme for PNR Klyshko's technique: a pulsed laser beam is used to pump a non-linear crystal in which take place SPDC. The heralding signal from DET1 announces the presence of the conjugated photon (idler) that is coupled in the single mode optical fibre and sent towards the TES based detector (DET2, identified by the dotted line) starting from the fibre end (b). DET1 and DET2 are gated by the laser trigger.

The typical output of a PNR detector is an histogram representing the relative frequency of detection events of a certain number of photons, see Fig 17.

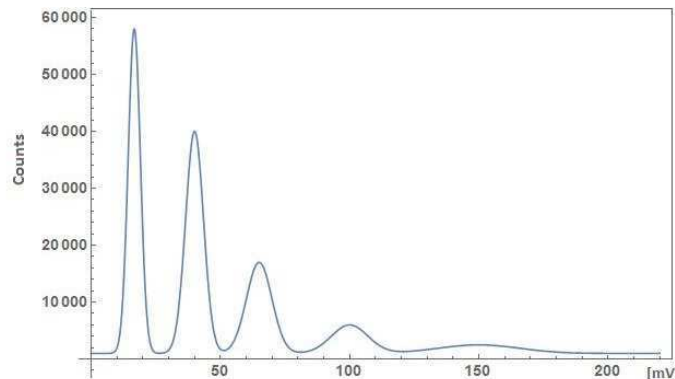


Figure 17. Figure report the typical output of a Transition Edge Detector (i.e. one of the most promising PNR detector). In abscissa we have the amplitude of the output signal and each peak correspond to a particular number of simultaneously detected photons.

To perform an absolute calibration it is necessary to acquire two separate measures, one in the presence of and one in the absence of heralding photons, obtaining two data

histograms. Starting from these histograms it is possible to estimate the probabilities of observing i photons in the presence and in the absence of the heralded photon, $P(i)$ and $\mathcal{P}(i)$.

Now, we have to consider the following quantities: ξ is the probability of having a true heralding count (i.e. not due to noise), γ is the overall quantum efficiency (including detector efficiency and channel losses), τ is the transmissivity of the optical channel from the crystal to the PNR detector, and η is the quantum efficiency of the detector itself. Therefore, we can write: $\gamma = \tau\eta$.

The probability of observing no photons on the PNR detector is the sum of the probability of non-detection of the heralded photons multiplied by the probability of having no accidental counts in the presence of a true heralding count and the probability of having no accidental counts in the presence of a heralding count due to noise counts:

$$P(0) = \xi[(1 - \gamma)\mathcal{P}(0)] + (1 - \xi)\mathcal{P}(0) \quad (101)$$

The probability of observing i counts is the sum of the joint probability of non-detection of the heralded photons and the probability of having i accidental counts, and the joint probability of detection of the heralded photons and the probability of having $i-1$ accidental counts both in the presence of a true heralding count, and the probability of having i accidental counts in the presence of a heralding count due to stray light or dark counts.

$$P(i) = \xi[(1 - \gamma)\mathcal{P}(i) + \gamma\mathcal{P}(i - 1)] + (1 - \xi)\mathcal{P}(i) \quad (102)$$

From Eq. (101) and Eq. (102) it is possible to derive the overall quantum efficiency of the channel in which the PNR detector is present. Note that, differently to original Klyshko's technique, there are several different independent ways to calculate the quantum efficiency, depending on the number of peaks that it is possible to observe in the histogram:

$$\gamma_0 = \frac{\mathcal{P}(0) - P(0)}{\xi\mathcal{P}(0)}, \quad \gamma_i = \frac{P(i) - \mathcal{P}(i)}{\xi[\mathcal{P}(i - 1) - \mathcal{P}(i)]}, \quad (103)$$

Each of these derivations of the quantum efficiency $\gamma(i)$ exploits a different number of simultaneously detected photons and can be calculated independently. However, all the $\gamma(i)$ represent the same physical quantity and should have the same value for a linear detector. Therefore, this extension of the Klyshko's technique allows checking the consistency of the detection model with data comparing different $\gamma(i)$.

Also in this case, to obtain the quantum efficiency of the detector as $\eta_{int} = \gamma/\tau$ it is necessary to estimate the losses τ independently.

Recently, a detailed theoretical analysis was performed about the possibility of extending the quantum correlations calibration technique to higher photon fluxes [193, 194]. Such studies allowed developing calibration techniques in the case of analogical bucket detectors using SPDC [195] and stimulated parametric down conversion [196].

8.3. Absolute calibration for analog spatial resolving detectors

The techniques described before are suitable for calibrating the so called bucket detectors, i.e. devices that collect the whole signal impinging on the sensor without any spatial resolution. Calibration techniques for spatial resolving detectors are essential for many applications of which imaging represents the most important. Due to their importance, in the following, we focus our attention on the Charge-Coupled Devices (CCD cameras), but, in principle, the technique described here can be applied to any spatial resolving detector that provide, point by point, an analogical signal proportional to the impinging light flux.

In the last years, quantum correlations were deeply explored in order to develop an absolute calibration technique for CCD cameras [197, 198, 199, 200]. In 2010, the first absolute calibration of a standard CCD camera was realized by exploiting bright squeezed vacuum [201] and, after several improvement, such technique reached a level of accuracy suitable for metrological application [202] and aligned with the state of the art of the absolute calibration of single photon detector with Klyshko's method.

Standard CCD cameras, i.e. without any avalanche electro-multiplication, are able to count the number of photo-electron generated in each pixels for a given exposure time. Therefore, their output is proportional to the intensity of adsorbed light (analogical regime).

There are two main sources of noise in CCD cameras: thermal noise and read noise. The thermal noise is due to charges generated by internal thermal excitations. It is proportional to the exposure time and it is strongly dependent by the temperature. Therefore, with a correct setting of this two parameters, thermal noise can be neglected for our purpose. Otherwise, the read noise is generated in the electronics reading process and it is independent by the exposure time and other physical parameters. Read noise contribution is not avoidable and, even if, for top-level devices its value is only few photoelectrons for frame, its presence implies that single photons can not be distinguished from the background.

Differently by bucket detectors, spatial resolving property of CCDs allows them to register the SPDC light emitted at several directions and for a long integration time. Therefore, a multi-mode treatment of the spatial distribution of SPDC emission is necessary. We can start from the considerations on SPDC exposed in chapter 4.4 to build an approximated model suitable for our purpose.

The calibration method is based on the measurement of statistical parameters between symmetric areas belonging to the twin beams, which in principle depend only by the transmission and detection efficiency. If we assume to have $\eta_1 = \eta_2 = \eta$ a good choices is the measured noise reduction factor σ_{det} defined in Eq.(59). That is depending by η in the following way:

$$\sigma_{det} \simeq 1 - \eta A \quad (104)$$

However, experimentally we have to consider that it is possible have an unbalancing in the efficiencies and as consequence it is not possible to use directly the noise reduction

factor to perform an absolute calibration. Therefore, we introduce a new parameter σ_α that compensate the unbalancing of the losses.

$$\sigma_\alpha \simeq \frac{1 + \alpha}{2} - \eta A \quad (105)$$

in which σ_α is defined as:

$$\sigma_\alpha = \frac{\langle \delta(\hat{n}_1 - \alpha \hat{n}_2)^2 \rangle}{\langle \hat{n}_1 + \alpha \hat{n}_i \rangle} \quad (106)$$

and where $\alpha = \langle \hat{n}_1 \rangle / \langle \hat{n}_2 \rangle$ is the measurable ratio between the beams intensities.

The quantity A , defined in Eq.60, is a geometrical parameter that takes into account the different modes contributions. In chapter 4.4, it is possible to find a detailed description of how to determine the parameter A , and how to minimise the misalignment between the correlated areas.

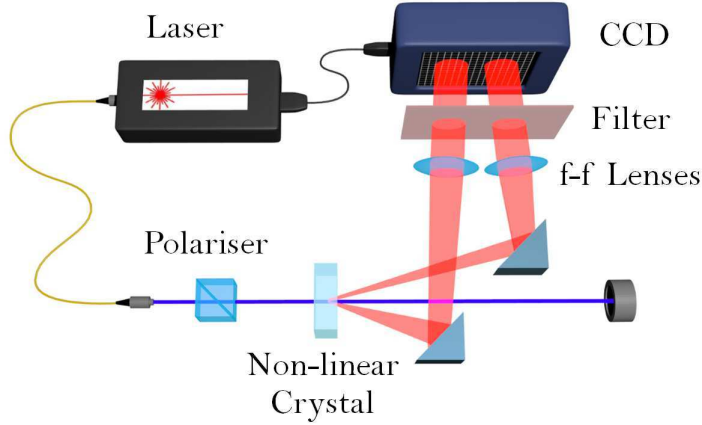


Figure 18. Schematic representation of an experimental apparatus for absolute calibration of spatial resolving detectors, like CCDs.

Notice that, the η obtained by inverting the equations 105 is a mean value over the whole area of detection \mathcal{A}_{det} . Therefore, it is not possible obtain a map of the quantum efficiency $\eta(\mathbf{x})$ of the active surface of the CCD. This aspect, maybe, is the most important limitation of these calibration techniques.

8.4. EMCCD as link between single photon level to high intense level

Electro-Multiplied CCDs (EMCCD) are cameras that are able of detecting single photon events with high quantum efficiency. This capability is achievable exploiting an electron multiplication structure built into the sensor that can be activated or not, giving the possibility to switch, from analog to single photon regime, using the same device.

In photon counting regime, each pixel of the EMCCD operates in Gaiger mode (as a click/no-click detector). This behaviour is achieved by applying a discriminating threshold T on the electron counts n_e at each pixel: a photon is detected if $n_e > T$. In

this regime, a selected detection area \mathcal{A}_{det} on the sensor can be considered as a non-linear photon number resolving detector, counting the number of incident photons on many pixels (spatial multiplexing) and acquiring many frames (time multiplexing).

By the measurement of spatially multimode quantum correlation in a squeezed vacuum it is possible to calibrate an EMCCD both in the analog regime and in the photon counting regime obtaining two different quantum efficiencies, indicated respectively with η_0 and $\eta(T)$. The quantum efficiency in single photon counting regime is strongly dependent by the threshold T .

The calibration of the analog quantum efficiency is already described in the previous section. Here we will describe how performing the calibration in photon counting regime and how it is possible to build a model of the detector that links η_0 to $\eta(T)$, as demonstrated in a recent experimental work [203].

First of all we need a model that describes the behaviour of $\eta(T)$ in function of several parameters that are possible to estimate experimentally.

The statistical distribution of the output counts of an EMCCD is well understood [204, 205]. For n photoelectrons at its input, the multiplication stage of each pixel provides a random number of electron counts x following the distribution:

$$\mathcal{P}(x|n) = \frac{x^{n-1} \exp(-x/g)}{g^n (n-1)!} \quad \text{for } n > 0; \quad (107)$$

$$\mathcal{P}(x|n) = \delta(x) \quad \text{for } n = 0; \quad (108)$$

where g is the multiplication gain. The total number of electron counts per pixel is due to the contribution of photoelectrons multiplication counts and to the noise counts. Therefore, the counts distribution at the output is the convolution of $\mathcal{P}(x|n)$ with the noise distribution:

$$P_{tot}(x|n) = \int_{-\infty}^{\infty} \mathcal{P}(y|n) P_{noise}(x-y) dy. \quad (109)$$

There are three most relevant noise contributions that are involved in EMCCD detection: read noise, dark current and spurious charges.

The read noise is generated by the on-chip output amplifier and follows a Gaussian distribution $P_{rn}(x; \mu, \sigma)$ where the mean value μ is the bias level of the read-out distribution and the standard deviation σ characterizes the fluctuation of read noise:

$$P_{rn}(x; \mu, \sigma) = \frac{1}{\sigma \sqrt{2\pi}} \exp \left[\frac{-(x - \mu)^2}{(2\sigma^2)} \right]. \quad (110)$$

this noise contribution is equivalent to the read noise in the analogical regime. The dark current is due to thermally generated charges and strongly depends on temperature and acquisition time. Even in this case, the camera parameters can be setted to have a negligible amount of dark current. A peculiarity of EMCCD operating in photon counting regime is the Clock Induced Charges (CIC) noise, also called spurious charges noise. CIC are created during the shift of the photoelectrons from the sensor to the

readout register. CIC generate an electron counts distribution $P_{sc}(x|n)$ that has the same behaviour of Eq. 107, but with gain g_{sc} lower than g :

$$P_{sc}(x|n) = \frac{x^{n-1} \exp(-x/g_{sc})}{g_{sc}^n (n-1)!}, \quad (111)$$

It is possible to set the camera parameters in order to have a negligible probability to generate more than one spurious charge per pixel. Therefore, the probability distribution of the electron counts, in the absence of illumination (i.e. without electrons generated by photon absorption), is given by:

$$P_{noise}(x) = (1 - p_{sc})P_{rn}(x) + p_{sc} \int_{-\infty}^{\infty} P_{rn}(y)P_{sc}(x - y|n = 1)dy, \quad (112)$$

where $P_{sc}(x|1) = \frac{e^{-x/g_{sc}}}{g_{sc}}$ is the distribution of electron counts generated by one spurious event and p_{sc} is the probability to have a spurious event. Therefore, the probability that a pixel clicks due to the noise is:

$$Noise(T) = \int_T^{\infty} P_{noise}(x)dx. \quad (113)$$

The next considerations are valid only in the regime in which the light level is sufficiently low to assume that no more than one photon per pixel is detected. The probability that a pixel clicks becomes:

$$P_{click} \simeq \eta_0 p_{ph} P_1(x \geq T) + (1 - p_{ph}) P_{noise}(x \geq T) \quad (114)$$

where η_0 is the probability that an incident photon generates a photo-electron and corresponds to the analog detection efficiency. Using a threshold sufficiently high to cut out the main part of the read noise ($T \geq 2\sigma + \mu$), we are sure that the probability to have a double click on the same pixel is negligible even considering all possible double event like: photon-photon, photon-noise, noise-noise. In this condition the probabilities are:

$$P_{click} \simeq \eta_0 p_{ph} P_1(x \geq T) + P_{noise}(x \geq T) \quad (115)$$

$$P_{true}(x \geq T) = \eta_0 p_{ph} P_1(x \geq T). \quad (116)$$

Hence we can measure the number of true counts, as $n_{true} = n_{click} - n_{noise}$.

$P_1(x)$ represents the electron counts distribution under the assumption that there is at most one photon per pixel, that there are no spurious counts and taking into account the contribution of the read noise:

$$P_1 = \int_{-\infty}^{\infty} \frac{1}{\sigma \sqrt{2\pi}} e^{-\frac{(y-\mu)^2}{2\sigma^2}} \mathcal{P}_1(x - y) dy, \quad (117)$$

where the distribution of electron counts generated by one photon is

$$\mathcal{P}_1(x) = \mathcal{P}(x|n = 1) = g^{-1} e^{-x/g}. \quad (118)$$

Now that we have a complete model of the statistical response of a EMCCD camera, it is possible reconstruct the behaviour of the quantum efficiency. The quantum efficiency, for a camera in single photon counting regime, is defined as:

$$\eta(T) = P_{true}(T)/p_{ph} = \eta_0 P_1(x \geq T), \quad (119)$$

where $P_{true}(T)$ is the probability that a pixel clicks ($x \geq T$) due to an incident photon Eq. (116) and p_{ph} is the probability to have an incident photon.

In principle, also in the case of an EMCCD operating in photon counting regime, it is possible to exploit the Klyshko's method to perform an absolute calibration of the quantum efficiency. However, there are two main practical reasons that prevent its use. First of all, Klyshko's technique needs a very low intensity illumination regime, (i.e. not more than one coincidence per frame). Unfortunately, in this illumination range the CIC noise becomes dominant, preventing any attempt to find true coincidence over a reasonable detection area. The second reason is that the read time of an EMCCD is much higher with respect to typical single-photon detectors, as a consequence the Klyshko's technique would be too much slow for practical applications.

The main difference between the Klyshko's twin-photon coincidence technique and the method used for EMCCD stems from the fact that we compared the number of detected photons in correlated areas in a large integration time, exploiting the technique developed for a CCD in the analog regime described in the section 8.3.

Also in this case it is possible to measure the noise reduction factor corrected by α like reported in Eq.s (106), but we have to take into account that in this case n_1 and n_2 represent the number of pixels that click and therefore they depend by the threshold T:

$$\sigma_\alpha(T) = \frac{\langle \delta(\hat{n}_1(T) - \alpha \hat{n}_2(T))^2 \rangle}{\langle \hat{n}_1(T) + \alpha \hat{n}_i(T) \rangle} \quad (120)$$

Such quantity satisfies the same relations with quantum efficiency as reported in Eq.s (105):

$$\sigma_\alpha(T) \simeq \frac{1 + \alpha}{2} - \eta(T)A \quad (121)$$

Therefore, there is the possibility to use the same absolute calibration technique, for the same device, both for the photon counting regime and the analogical regime. Moreover, the model in Eq.(119) link the quantum efficiencies η_0 and $\eta(T)$, providing a radiometric link between the low illumination range to the mesoscopic and to the macroscopic range. This represents an important step in the field of quantum radiometry, in particular because it allow the metrological traceability of measurements at the few-photon level, that is essential for most of the emerging quantum technologies.

In this last chapter we have focused our attention on the EMCCD cameras, that are, maybe, the most diffuse spatial resolving devices allowing single photon counting. However, there are others kind of spatial resolving detectors that are able to working in this regime. For example, an important commercial devices are the Intensified CCD for which have been developed similar absolute calibration techniques [206] and klyshko's calibration techniques [207] . Alternatively have been recently developed new kind of spatial resolving detectors that exploit arrays of true "click/no click" single photon detectors [208]. This last kind of devices, largely used in recent quantum optics experiments [209, 210], can exploit directly the calibration techniques based on noise reduction factor σ and the correlation C without the need to develop a models describing the detector output statistic like in tha case of EMCCDs and Intensified CCDs.

Conclusions

Quantum correlations emerged as a fundamental tool for developing quantum technologies.

In particular, quantum correlations of the optical field are the most exploited resource for these new technologies, whose applications ranges from quantum imaging and sensing to quantum communication and quantum computation.

In this review paper we have summarized the main properties of photon statistics and photon number correlations of technologically relevant optical fields, describing in some detail the use of twin beams in a few quantum enhanced protocols. Our main message is that the relatively easy production of these last states and their demonstrated advantages in various protocols make them a fundamental tool for overpassing the death valley between proof of principle experiments and commercial systems. They will therefore represent a source of the utmost importance for the approaching second quantum revolution.

acknowledgements

We acknowledge the support of the MIUR Project *Premiale P5* and of the John Templeton Foundation (*Grant ID 43467*). The opinions expressed in this publication are those of the authors and do not necessarily reflect the views of the John Templeton Foundation.

References

- [1] Genovese M 2005 *Phys. Rep.* **413** and ref.s therein.
- [2] M. Genovese 2009 *Adv. Sci. Lett.* **2** 303
- [3] Moreva E et al. 2014 *Phys. Rev. A* **89** 052122
- [4] Giovannetti V, Lloyd S, Maccone L 2004 *Science* **306** 1330-6.
- [5] Huang Z, Macchiavello C and Maccone L 2016 *Phys. Rev. A* **94** 012101
- [6] N.Gisin and R. Thew 2007 *Nature Photonics* **1**, 165-171
- [7] U. Vazirani and T. Vidick 2014 *Phys. Rev. Lett.* **113** 140501
- [8] Taylor M A, Bowena WP. 2016 *Physics Reports* **615** 1-59.
- [9] Wu J, Liu F, Shen Y, Cao J and Silbey R J 2010 *New J. Phys.* **12** 105012
- [10] Giorgi G L, Roncaglia M, Raffa F A, Genovese M 2015 *Annals of Physics* **361** 7281
- [11] D. Gatto Monticone et al. 2014 *Phys. Rev. Lett.* **113** 143602 ; Thiel C et al 2007 *Phys. Rev. Lett.* **99** 133603; Pope F. et al. 2016 *Quantum Metrology* **3** 20; ArXiv 1504.05435 and ref.s therein.
- [12] Kolobov M I. 2007 *Quantum Imaging* New York: Springer
- [13] Genovese M 2016 *Journal of Optics* **18** 7
- [14] Simon D S, Jaeger G, Sergienko A V, 2017, “Quantum Metrology, Imaging and Communication”, Springer, New York, ISBN: 978-3-319-46549-4
- [15] Huelga S F, Macchiavello C, Pellizzaro T, Ekert A K 1997 *Phys. Rev. Lett.* **79** 3865
- [16] Boto A, Kok P et al. 2000 *Phys. Rev. Lett.* **85** 2733
- [17] Holland M J and Burnett K, 1993 *Phys. Rev. Lett.* **71**, pp. 13551358
- [18] Campos R A, Gerry C C and Benmoussa A 2003 *Phys. Rev. A* **68** 023810
- [19] Ono T, Okamoto R, Takeuchi S. 2013 *Nature Commun.* **4** 2426

- [20] Israel Y, Rosen S, Silberberg Y 2014 *Phys. Rev. Lett.* **112** 103604
- [21] Wolfgramm F, Vitelli C, Beduini F A, Godbout N, Mitchell M W 2013 *Nature Photonics* **7** 2832
- [22] Crespi A, Lobino M, Matthews J, Politi A, Neal C, Ramponi R, Osellame R, O'Brien J. 2012 *Appl. Phys. Lett.* **100** 233704
- [23] D'Angelo M et al. 2001 *Phys. Rev. Lett.* **87** 013602
- [24] Vitelli C, Spagnolo N, Sciarrino F and De Martini F 2009 *JOSA B* **5** 892
- [25] Jachura M et al. 2016 *Nature Comm.* **7** 11411
- [26] Demkowicz-Dobrzański R, Koodyski J, Gu M. 2012 *Nature Commun* **3** 1063.
- [27] Giovannetti V and Maccone L 2012 *Phys. Rev. Lett.* **108** 210404
- [28] Demkowicz-Dobrzański R, Jarzyna M, Koodyski J. J. 2015 *Prog Opt* **60** 345
- [29] Mankei Tsang 2013 *New Journal of Physics* **15** 073005
- [30] Ferraro A, Olivares S and Paris M G A arXiv:quant-ph/0503237
- [31] Andersen U, Gehring T, Marquardt C and Leuchs G 2016 *Phys. Script.* **91**, 053001
- [32] Schnabel R, arXiv:1611.03986v1 [quant-ph] 12 Nov 2016
- [33] Olivares S, Popovic M, Paris M G A 2016 *Quantum Measurements and Quantum Metrology* **3** 38
- [34] Mehmet M, Ast S, Eberle T, Steinlechner S, Vahlbruch H, Schnabel R. 2011 *Opt. Exp.* **19** 25763.
- [35] Caves CM. 1981 *Phys. Rev. D* **23** 1708
- [36] Abadie J et al. 2001 *Nature Physics* **7** 2083
- [37] Taylor MA, Janousek J, Knittel DJ, Hage B, Bachor HA, Bowen WP 2013 *Nature Photonics* **7** 229233
- [38] Taylor MA, Janousek J, Daria V, Knittel DJ, Hage B, Bachor HA, Bowen WP 2014 *Phys Rev X* **4** 011017
- [39] Ruo Berchera I et al. 2013 *Phys. Rev. Lett.* **110** 213601
- [40] Souza L A M et al. 2015 *Phys. Rev. Lett.* **92** 052122
- [41] Lopaeva E D, Ruo Berchera I, Degiovanni I P, Olivares S, Brida G and Genovese M 2013 *Phys. Rev. Lett.* **110** 153603
- [42] Corzo NV, Marino AM, Jones KM, Lett PD. 2012 *Phys. Rev. Lett.* **109** 043602
- [43] Boyer V, Marino AM, Pooser RC, Lett PD. 2008 *Science* **321** 5888.
- [44] Adenier G et al. 2016 *International Journal of Quantum Information* **14** 1640014
- [45] Samantaray N, Ruo-Berchera I, Meda A, Genovese M 2016 *Light. Sci. & App.* (to appear), arXiv:1612.06169 [quant-ph].
- [46] Belinskii A and Klyshko D 1994 *Sov. Phys. JETP* **78** 259
- [47] Pittman T B, Shih Y H, Strekalov D V 1995 *Phys. Rev. A* **52** R3429R3432
- [48] Zwinkels J C, Ikonen E, Fox N P, Ulm G Rastello M L 2010 *Metrologia* **47** R15-R32
- [49] Zel'Dovich, Ya B and Klyshko D N 1969 *JETP. Lett.* **9** 40
- [50] Polyakov S V and Migdall A L 2007 *Opt. Express* **15** 1390
- [51] Glauber R J 1965 *Quantum Optics and Electronics* (C. de Witt, A. Blandin, and C. Cohen-Tannoudji, Gordon and Breach, New York).
- [52] Arecchi F T 1965 *Phys. Rev. Lett.* **15** 912
- [53] Shapiro J H 2012 *Quantum Information Processing* **11** 949993.
- [54] Glauber R J 1963 *Phys. Rev.* **131** 2766
- [55] Sudarshan E C G 1963 *Phys. Rev. Lett.* **10** 277
- [56] Davidovich L 1996 *Rev. Mod. Phys.* **68** 127
- [57] Demkowicz-Dobrzański R, Jarzyna M, Kołodyński L 2012 **60** 345435.
- [58] Shapiro J H 2009 *IEEE J. Sel. Top. Quantum Electron.* **15** 15471569.
- [59] Shapiro J H 2010 *IEEE J. Sel. Top. Quantum Electron.* **16** 698.
- [60] Yuen H P, Shapiro J H 1980 *IEEE Trans. Inf. Theory* **26** 7892.
- [61] Gagliardi R M, Kamp S 1976 *Optical Communications*, (NewYork: Wiley).
- [62] Gowar J 1984 *Optical Communication Systems (Optoelectronics)* (NewYork: Prentice-Hall).
- [63] Palms J M, Venugopala Rao P, Wood R E 1969 *Nuclear Instruments and Methods* **76** 1.
- [64] Mandel L 1979 *Optics Lett.* **4** 7.

- [65] Jedrkiewicz O, Jiang YK, Brambilla E, Gatti A, Bache M, Lugiato LA, Di Trapani P. 2004 *Phys Rev Lett* **93** 243601.
- [66] Mosset A, Devaux F, Lantz E 2005 *Phys Rev Lett* **94** 223603.
- [67] Blanchet JL, Devaux F, Furfaro L, Lantz E 2008 *Phys. Rev. Lett.* **101** 233604.
- [68] Bondani M, Allevi A, Zambra G, Paris M, Andreoni 2007 *Phys. Rev. A* **76** 013833.
- [69] Perina J Jr, Hamar M, Michalek V, Haderka O 2012 *Phys. Rev. A* **85** 023816.
- [70] Iskhakov TS, Usenko VC, Andersen UL, Filip R, Chekhova MV, Leuchs G 2016 *Opt. Lett.* **41** 2149-2152.
- [71] Iskhakov TS, Usenko VC, Filip R, Chekhova MV and Leuchs G 2016 *Phys. Rev. A* **93** 043849
- [72] Ishakov TS, Chekhova MV, Leuchs G 2009 *Phys. Rev. Lett.* **102** 183602.
- [73] Tapster P R, Seward S F, Rarity J G. 1991 *Phys. Rev. A.* **44** 3266.
- [74] Brida G, Degiovanni IP, Genovese M, Rastello ML, Berchera IR 2010 *Opt Express* **18** 20572-20584.
- [75] Lamperti M et al 2014 *Int. J. Quantum Inform.* **12** 1461017
- [76] Sekatski P, Sangouard N, Bussi eres F, Clausen C, Gisin N, Zbinden H 2012 *J. Phys. B* **45** 124016.
- [77] Avella A 2015 *Journal of Advanced Physics* **4** 252-262
- [78] Ruo-Berchera I 2009 *Advanced Science Letters* **2** 407-429
- [79] Burnham D C and Weinberg D L 1970 *Phys. Rev. Lett.* **25** 84
- [80] Sergienko AV, Atature M, Walton Z, Jaeger G, Saleh BEA and Teich M C 1999 *Phys. Rev. A* **60** R2622(R)
- [81] Jennewein T, Simon C, Weihs G, Weinfurter H, and Zeilinger A 2000 *Phys. Rev. Lett.* **84** 4729
- [82] Adachi Y, Yamamoto T, Koashi M, and Imoto N 2007 *Phys. Rev. Lett.* **99** 180503
- [83] Avella A, Brida G, Degiovanni IP, Genovese M, Gramegna M, Traina P 2010 *Phys. Rev. A* **82** 062309
- [84] Brida G, Cavanna A, Degiovanni I P, Genovese M, Traina P 2012 *Laser Physics Letters* **9** 247252
- [85] R. All eume 2014 *Theoretical Computer Science* **560** 62-81
- [86] Bouwmeester D, Pan J, Mattle K, Eibl M, Weinfurter H and Zeilinger A 1997 *Nature* **390** 575-579
- [87] Sansoni L, Sciarrino F, Vallone G, Mataloni P, Crespi A, Ramponi R and Osellame R *Phys. Rev. Lett.* **108** 010502
- [88] Sansoni L, Sciarrino F, Vallone G, Mataloni P, Crespi A, Ramponi R and Osellame R 2010 *Phys. Rev. Lett.* **105** 200503
- [89] Avella A, Gramegna M, Shurupov A, Brida G, Chekhova M, Genovese M 2014 *Phys. Rev. A* **89** 023808
- [90] Brida G, Genovese M, Chekhova M V, and Krivitsky L A 2008 *Phys. Rev. A* **77** 015805
- [91] Brida G, Genovese M, Krivitsky L A et al. 2007 *Laser Phys.* **17** 567
- [92] Brida G, Chekhova M V, Degiovanni I P, Genovese M, Kitaeva G K, Meda A and Shumilkina O A 2009 *Phys. Rev. Lett.* **103** 193602
- [93] Bogdanov Y I, Chekhova M V, Kulik S P, Maslennikov G A, Oh C H, Tey M K 2004 *arXiv:quant-ph/0411192*
- [94] Lemos G B, Borish V, Cole G. D., Ramelow S, Lapkiewicz R. and Zeilinger A. 2014 *Nature* **512** 409412
- [95] Kalashnikov D A, Paterova A V, Kulik S P and Krivitsky L. A. 2016 *Nature Photonics* **10** 98101
- [96] Sciarrino F, Vallone G, Milani G, et al. 2011 *The European Physical Journal Special Topics* **199** 111-125
- [97] Avella A, Genovese M 2015 *Journal of Advanced Physics* **4** 233-235
- [98] Giustina M, Versteegh M, Wengerowsky A, et al. 2015 *Phys. Rev. Lett.* **115** 250401
- [99] Brida G, Cagliero E, Falzetta G, Genovese M, Gramegna M, and Predazzi E 2003 *Phys. Rev. A* **68** 033803
- [100] Cole R 2015 *Cell Adh. Migr.* **8** 5
- [101] Tapster P R, Seward S F, Rarity J G 1991 *Phys. Rev. A* **44** 3266.
- [102] Moreau P A, Chesterking J S, Whittaker R, Joshi S K, Birchall P, McMillan A, Rarity J G, Matthews J C F 2016 *arXiv:1611.07871v1*

- [103] Brambilla E, Caspani L, Jedrkiewicz O, Lugiato L A, and Gatti A 2008 *Phys. Rev. A* **77** 053807
- [104] Brida G et al. 2009 *Phys. Rev. Lett.* **102** 213602
- [105] Brida G, Genevese M, Ruo-Berchera I *Nature Photon* **4** 227 - 230
- [106] Gerry C C and Knight P 2005 *Introductory quantum optics*, Cambridge university press.
- [107] Lloyd S 2008 *Science* **321** 1463.
- [108] Tan S H, Erkmen B I, Giovannetti V, Guha S, Lloyd S, Maccone L, Pirandola S, and Shapiro J H 2008 *Phys. Rev. Lett.* **101** 253601.
- [109] Shapiro J H and Lloyd S 2009 *New J. Phys.* **11** 063045.
- [110] Zhang S L, Guo J S, Bao W S, Shi J H, Jin C H, Zou X B, and Guo G C, 2014 *Phys. Rev. A* **89** 062309
- [111] Guha S and Erkmen B I 2009 *Phys. Rev. A* **80** 052310
- [112] Zhang Z, Mouradian S, Wong F N C, and Shapiro J H 2015 *Phys. Rev. Lett.* **114** 110506
- [113] Zhang Z, Tengner M, Zhong T, Wong F N C, and Shapiro J H 2013 *Phys. Rev. Lett.* **111** 010501
- [114] Shapiro J H 2009 *Phys. Rev. A* **80** 022320
- [115] Barzanjeh S, Guha S, Weedbrook C, Vitali D, Shapiro J H, and Pirandola S 2015 *Phys. Rev. Lett* **114** 080503
- [116] Lopaeva E D, Ruo Berchera I, Degiovanni I P, Olivares S, Brida G, and Genovese M 2013 *Phys. Rev. Lett.* **110** 153603
- [117] Lopaeva E D, Ruo-Berchera I, Olivares S, Brida G, Degiovanni I P, and Genovese M 2014 *Phys. Scr.* T160 014026
- [118] Ragy S, Ruo-Berchera I, Degiovanni I P, Olivares S, Paris M G A, Adesso G, and Genovese M 2014 *J. Opt. Soc. Am. B* 2045
- [119] Simon S et al 2014 *Int. Journ. Quant. Inf.* **12** 1430004
- [120] Lugiato L A et al 2002 *J. Opt. B* **4** S176
- [121] Kolobov M I 2007 *Quantum Imaging* (New York: Springer)
- [122] Treps N, Grosse N, Bowen W P, Fabre C, Bachor H A and Lam P K 2003 *Science* **301** 5635 940
- [123] Boyer V, Marino A M, Pooser R C and Lett P D 2008 *Science* **321** 544
- [124] Brida G, Genovese M and Ruo Berchera I 2010 *Nature Photonics* **4** 227
- [125] Brida G et al. 2011 *Phys. Rev. A* **83** 063807
- [126] Aspden R S et al. 2013 *New Journ. Phys.* **15** 073032
- [127] Yu W et al. 2014 *Opt. Lett.* **22** 7133
- [128] Gatti A, Brambilla E, Bache M, and Lugiato L A 2004 *Phys. Rev. Lett.* **93** 093602
- [129] Bennink R S, Bentley S J, Boyd R W 2002 *Phys. Rev. Lett.* **89** 113601
- [130] Ferri F, Magatti D, Gatti A, Bache M, Brambilla E, and Lugiato L A 2005 *Phys. Rev. Lett.* **94** 183602
- [131] Valencia A, Scarcelli G, D'Angelo M, and Shih Y 2005 *Phys. Rev. Lett.* **94** 063601
- [132] Chen X, Agafonov I N, Luo K, Liu Q, Xian R, Chekhova M V, Wu L 2010 *Opt.lett.* **35** 1166-1168
- [133] Zhai Y, Chen X, Zhang D, Wu L 2005 *Phys. Rev. A* **72** 043805
- [134] Liu X, Chen X, Yao X, Yu W, Zhai G, Wu L 2014 *Opt.Lett.* **39** 002314
- [135] Gong W and Han S 2011 *Opt.Lett.* **36** 000394
- [136] Bina M, Magatti D, Molteni M, Gatti A, Lugiato L A, and Ferri F 2013 *Phys. Rev. Lett.* **110** 083901
- [137] Meyers R E, Deacon K S, Tunick A D , Shih Y 2012 *Appl. Phys. Lett.* **100** 061126
- [138] Dixon P B et al. 2011 *Phys. Rev. A* **83** 051803(R)
- [139] Meda A, Caprile A, Avella A, Ruo Berchera I, Degiovanni I P, Magni A and Genovese M 2015 *Appl. Phys. Lett.* **106** 262405
- [140] Meyers R, Deacon K S, Shih Y 2008 *Phys. Rev. A* **77** 041801(R)
- [141] Meyers R E, Deacon K S 2010 *ARL. Proc. SPIE* 78150I
- [142] Shapiro J H 2008 *Phys. Rev. A* **78** 061802(R)
- [143] Bromberg Y, Katz O, Silberberg Y 2009 *Phys. Rev. A* **79** 053840
- [144] Katz O, Bromberg Y, Silberberg Y 2009 *Appl. Phys. Lett.* **95** 131110

- [145] Rubin M H, Shih Y 2008 *Phys. Rev. A* **78** 033836
- [146] Chan K W C , O'Sullivan M N , Boyd R.W 2009 *Phys. Rev. A* **79** 033808
- [147] Karmakar S, Shih Y 2010 *Proc. SPIE* 78150R
- [148] Chan K W C, O'Sullivan M N, Boyd R W 2009 *Opt. Express* **18** 55625573
- [149] Bache M, Brambilla E, Gatti A, Lugiato L A 2004 *Phys. Rev. A* **70** 023823
- [150] Morris P A, et al. 2015 *Nature Communications* **10** 1038
- [151] Brida G, Chekhova M V, Fornaro G A , Genovese M, Lopaeva E D, and Ruo Berchera I 2011 *Phys. Rev. A*. **83** 063807
- [152] Polyakov S V and Migdall A L 2009 *Journal of Modern Optics* **56** 1045-1052
- [153] O'Brien J L 2007 *Science* **318** 1567-1570
- [154] Lo HK, Curty M and Tamaki K 2014 *Nature Photonics* **8** 595604
- [155] Vahlbruch H, Mehmet M, Danzmann K, and Schnabel R 2016 *Phys. Rev. Lett.* **117** 110801
- [156] Bohmann M, Kruse R, Sperling J, Silberhorn C, Vogel W 2016 arXiv:1611.04779 [quant-ph]
- [157] Luis A and Sanchez-Soto 1999 *Phys. Rev. Lett.* **83** 3573
- [158] Fiurasek J 2001 *Phys. Rev. A* **64** 024102
- [159] D'Ariano G M, Maccone L and Lo Presti P. 2004 *Phys. Rev. Lett.* **93** 250407
- [160] Lundeen J S, Feito A, Coldenstrodt-Ronge H, Pregnell K L, Silberhorn C, Ralph T C, Eisert J, Plenio M B, and Walmsley I A 2009 *Nat. Phys.* **5**, 27
- [161] Mingolla M G, Piacentini F, Avella A, Gramegna M, et. al. 2015 *Quantum Matter* **4** 200-212
- [162] Piacentini F, Levi M P, Avella A, Lpez M, Kck S, Polyakov S V, Degiovanni I P, Brida G and Genovese M 2015 *Opt. Lett.* **40** 1548-1551
- [163] Brida G, Ciavarella L, et al. 2012 *New Journal of Physics*, **14**
- [164] Brida G, Ciavarella L, et al. 2012 *Phys. Rev. Lett.* **108** 253601
- [165] Bogdanov Y I, Brida G, Genovese M, Kulik S P, Moreva E V and Shurupov A P 2010 *Phys. Rev. Lett.* **105** 010404
- [166] Piacentini F, Avella A, Traina P, Lolli L, Taralli E, et al. 2016 *Quantum Meas. Quantum Metrol.* **3** 2731
- [167] Zeldovich B Y and Klyshko D N 1968 *Sov. Phys. J. Exp. Theor. Phys. Lett.* **9** 40
- [168] Burnham D C and Weinberg D L 1970 *Phys. Rev. Lett.* **25** 84
- [169] Kwiat P G, Steinberg A M, Chiao R Y, Eberhard P H, and Petroff M D 1994 *Appl. Opt.* **33** 10
- [170] Migdall A 1999 *Phys. Today* **52** 41
- [171] Brida G, Genovese M and Novero C 2000 *J. Mod. Opt.* **47** 2099
- [172] Brida G, Castelletto S, Degiovanni I P, Genovese M, Novero C, and Rastello M L 2000 *Metrologia* **37** 5
- [173] Cheung J Y, Chunnillall C J, Porrovecchio G, Smid M, and Theocharous E 2011 *Opt. Express* **19** 20347
- [174] Perina J, Haderka O, Michlek V and Hamar M 2012 *Optics Letters* **37** 2475-2477
- [175] Brida G and et al. 2000 *Metrologia* **37** 624
- [176] Brida G and et al. 2006 *Laser Physics letters* **3** 115
- [177] Brida G, Genovese M, Gramegna M, Rastello M L, Chekhova M, and Krivitsky L 2005 *Journal of the Optical Society of America B* **22** 488-492
- [178] Hadfield R H 2009 *Nature Photon* **3** 696-705
- [179] Silberhorn C, 2007 *Contemp. Phys.* **48** 143156
- [180] Jiang L A, Dauler E A, and Chang J T 2007 *Phys. Rev. A* **75** 062325
- [181] Divochiy A, Marsili F, Bitauld D, et al 2008 *Nature Photon.* **2** 302306
- [182] Achilles D, Silberhorn C, Sliwa C, Banaszek K, and Walmsley I A 2003 *Opt. Lett.* **28** 2387-2389
- [183] Fitch M J, Jacobs B C, Pittman T B, and Franson J D 2003 *Phys. Rev. A* **68** 043814
- [184] Zambra G, Bondani M, Spinelli A S, Paleari F, and Andreoni A 2004 *Rev. Sci. Instrum.* **75** 2762
- [185] Bondani M, Allevi A, and Andreoni A, 2009 *Adv. Sc. Lett.* **2** 463468
- [186] Morton G A 1949 *RCA Rev.* **10** 525
- [187] Ramilli M, Allevi A, Chmill V, Bondani M, Caccia M, and Andreoni A 2010 *J. Opt. Soc. Am. B*

27 852-862

- [188] Kim K, Takeuchi S, Yamamoto Y, and Hogue H H 1999 *Appl. Phys. Lett.* **74** 902
- [189] Waks E, Inoue K, Oliver W D, Diamanti E, and Yamamoto Y 2003 *IEEE J. Sel. Top. Quantum Electron* **9** 15021511
- [190] Irwin K D and Hilton G C 2005 *Topics Appl. Phys.* **99** 63149.
- [191] Hao L, Macfarlane J C, Lam S K H, Foley C P, Josephs-Franks P and Gallop J C 2005 *IEEE Trans. Appl. Superconductivity* **15** 514
- [192] Avella A, Brida G, Degiovanni I P, Genovese M, Gramegna M, Lolli L, Monticone E, Portesi C, Rajteri M, Rastello M L, Taralli E, Traina P and White M 2011 *Opt. Express* **19** 23249
- [193] Brida G, Chekhova M, Genovese M, Penin A, Rastello M L, and Ruo-Berchera I 2007 *IEEE Transactions on Instrumentation and Measurement* **56** 2
- [194] Brida G, Genovese M, Ruo-Berchera I, Chekhova M, and Penin A 2006 *J. Opt. Soc. Am. B* **23** 21852193 (2006).
- [195] Perina J, Haderka O, Allevi A and Bondani M 2014 *Appl. Phys. Lett.* **104** 041113
- [196] Brida G, Chekhova M, Genovese M, and Ruo-Berchera I 2008 *Opt. Express* **16** 1255012558
- [197] Brida G, Chekhova M, Genovese M, Penin A, and Ruo-Berchera I 2006 *J. Opt. Soc. Am. B* **23** 2185
- [198] Brida G, Chekhova M, Genovese M, and Ruo Berchera I 2008 *Opt. Express* **16** 12550
- [199] Brida G, Chekhova M, Genovese M, Rastello M L and Ruo-Berchera I 2009 *J. Mod. Opt.* **56** 401
- [200] Ruo Berchera I 2009 *Adv. Sci. Lett.* **2** 407
- [201] Brida G, Degiovanni I P, Genovese M, Rastello M L, and Ruo Berchera I 2010 *Opt. Express* **18** 20572-20584
- [202] Meda A, Ruo-Berchera I, Degiovanni I P, Brida G, Rastello M L, and Genovese M 2014 *Appl. Phys. Lett.* **105** 101113
- [203] Avella A, Ruo-Berchera I, Degiovanni I P, Brda G AND Genovese M 2016 *Optics Letters* **41** 1841
- [204] Hirsch M, Wareham R J, Martin-Fernandez M L, Hobson M P and Rolfe D J 2013 *PLoS One*. **8** 1
- [205] Lantz E, Blanchet J, Furfaro L and Devaux F 2008 *Mon. Not. R. Astron. Soc.* **386** 22622270
- [206] Haderka O, Perina J, Michalek V, Hamar M 2014 *JOSA B* **31** 10
- [207] Qi L, Just F, Leuchs G and Chekhova M V 2016 *Opt. Express* **24** 26444-26453
- [208] Villa F et al. 2014 *IEEE J. Sel. Top. Quantum Electron.* **20** 364
- [209] Piacentini F, Avella A, Levi MP, Lussana R, Villa F, Tosi A, Zappa F et al. 2016 *Phys. Rev. Lett.* **116** 180401
- [210] Piacentini F, Avella A, Levi MP, Gramegna M, Brida G, Degiovanni IP et al. 2016 *Phys. Rev. Lett.* **117** 170402